nature neuroscience

Supplementary information https://doi.org/10.1038/s41593-024-01800-6

Autism spectrum disorder variation as a computational trade-off via dynamic range of neuronal population responses

In the format provided by the authors and unedited

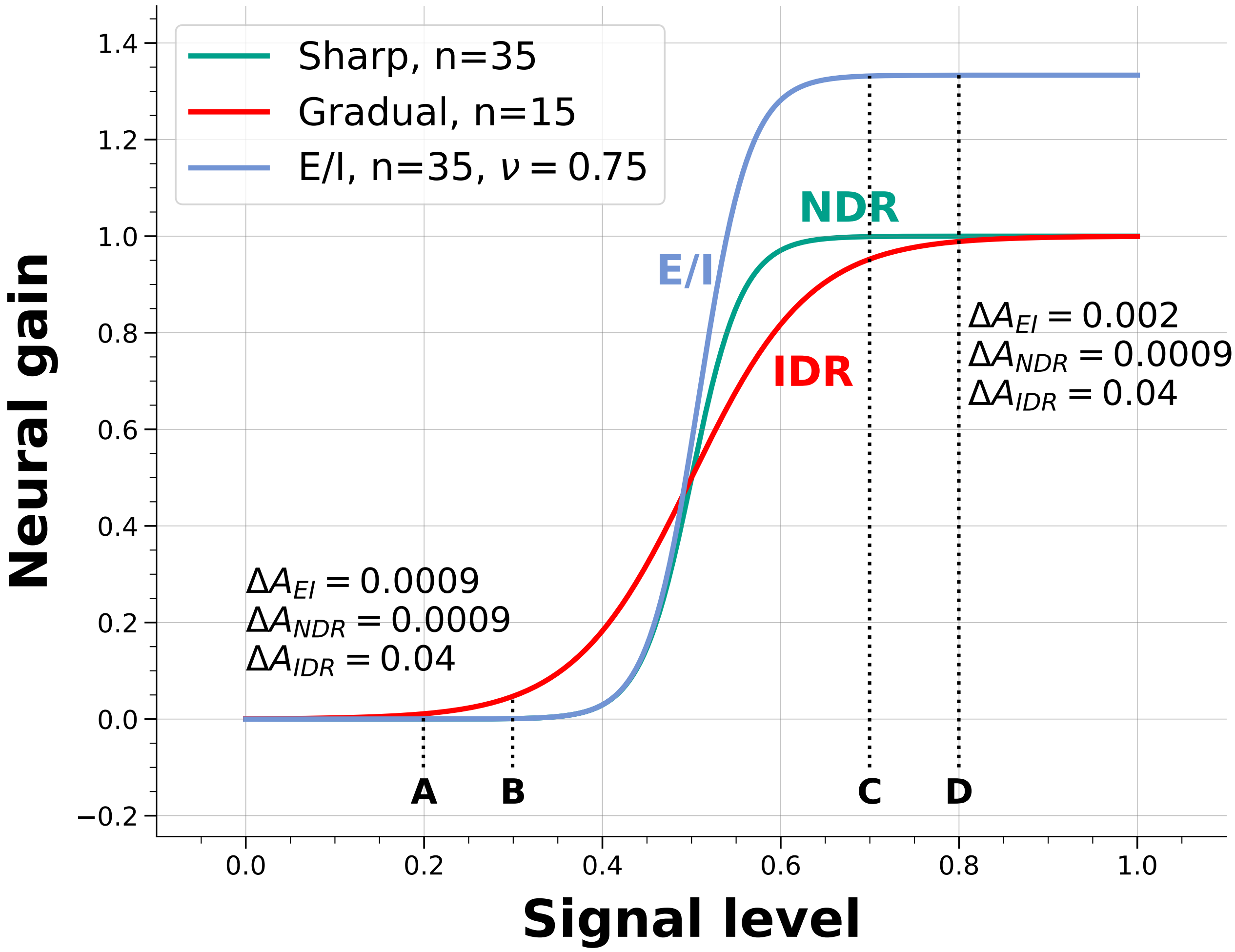

Supplementary Figure 1: Replication of Figure 1 in the main text using the logistic function sigmoid $\frac{1}{\nu+e^{-n(x-k)}}$

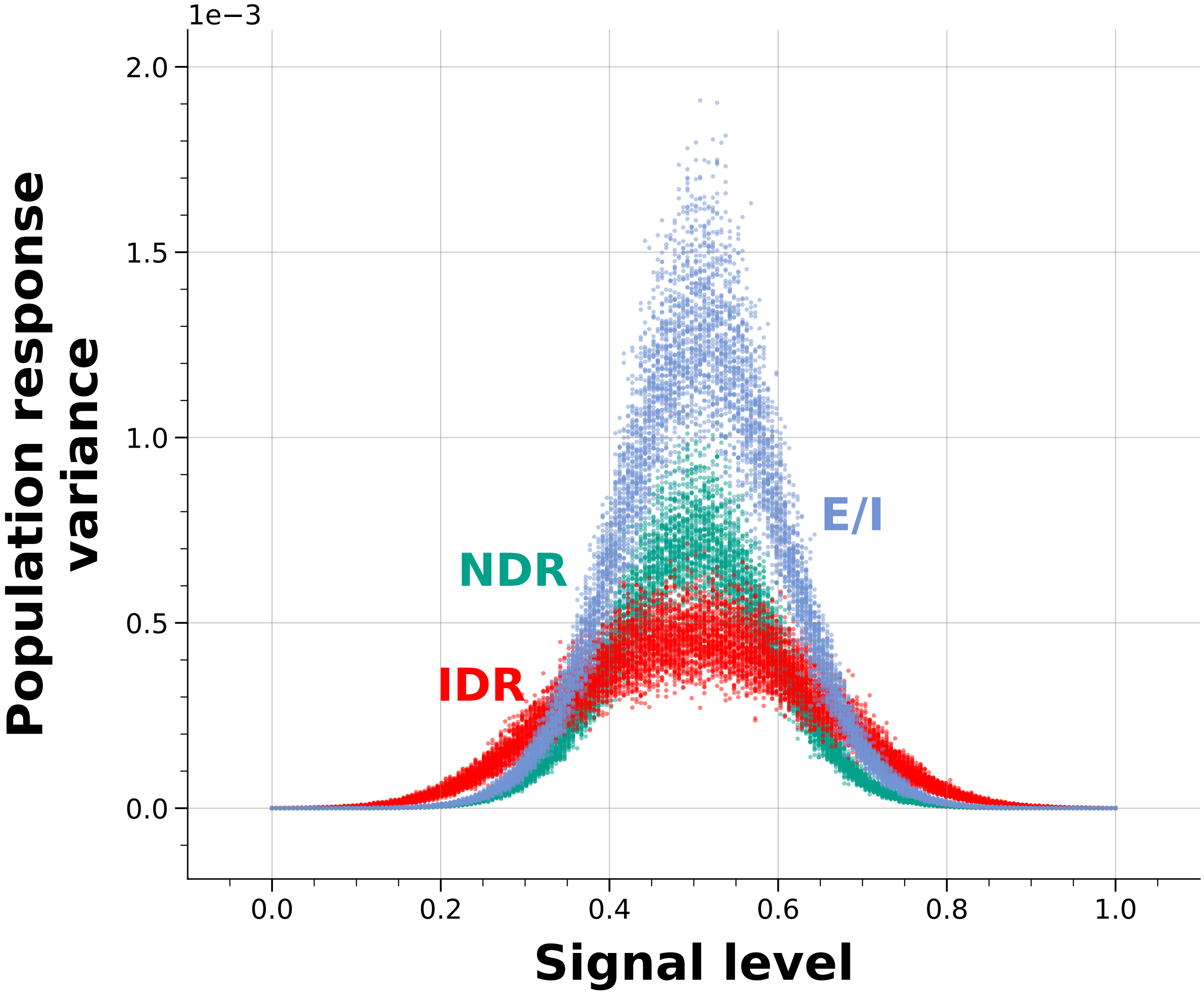

Supplementary Figure 2: Replication of Figure 2 in the main text using the logistic function sigmoid $\frac{1}{\nu+e^{-n(x-k)}}$

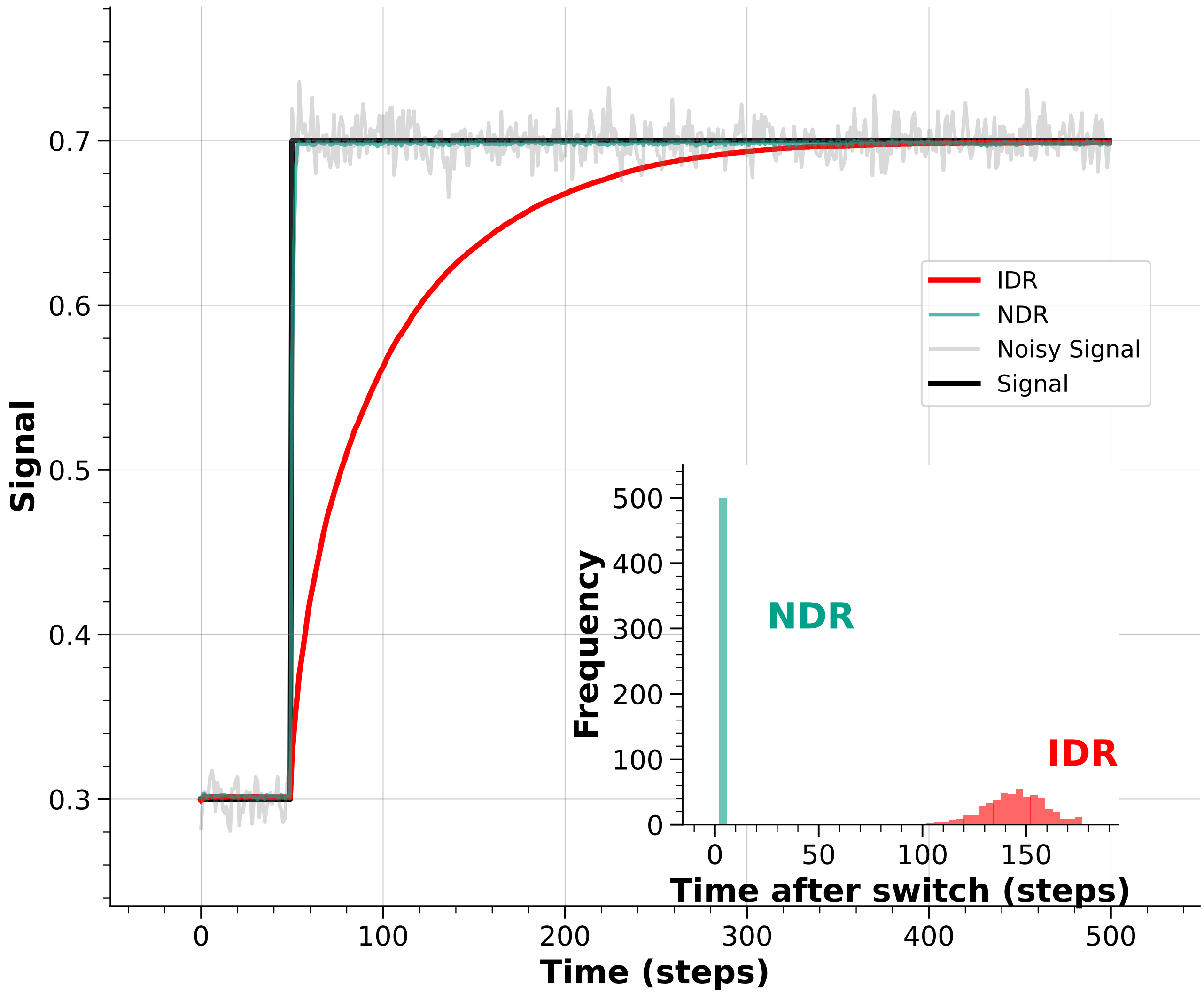

Supplementary Figure 3: Replication of Figure 3 panel A and inset in the main text using the logistic function sigmoid $\frac{1}{\nu+e^{-n(x-k)}}$. Two-sided Wilcoxon signed-rank test for $RT_{IDR} > RT_{NDR}$, $W = 0$, $p < 10^{-5}$)

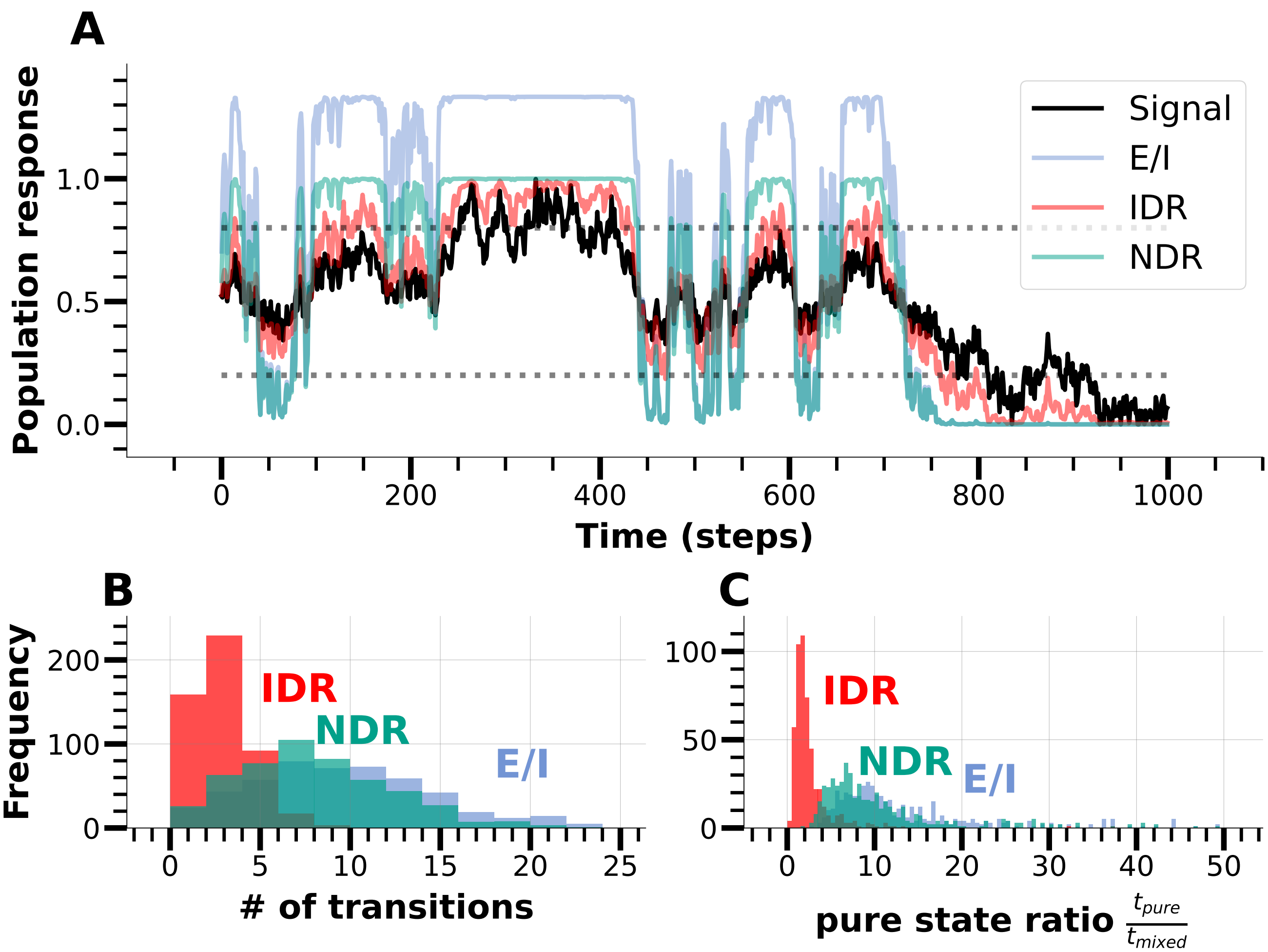

Supplementary Figure 4: Replication of Figure 4 in the main text using the logistic function sigmoid $\frac{1}{\nu+e^{-n(x-k)}}$

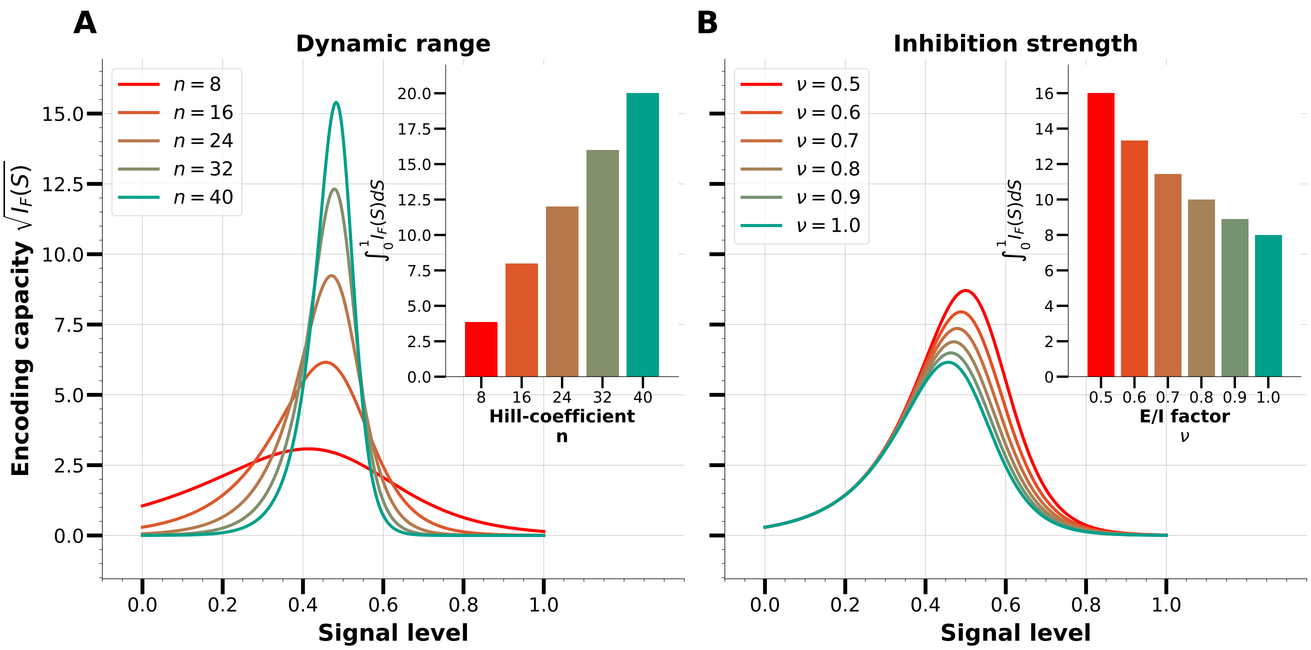

Supplementary Figure 5: Replication of Figure 6 in the main text using the logistic function sigmoid $\frac{1}{\nu+e^{-n(x-k)}}$

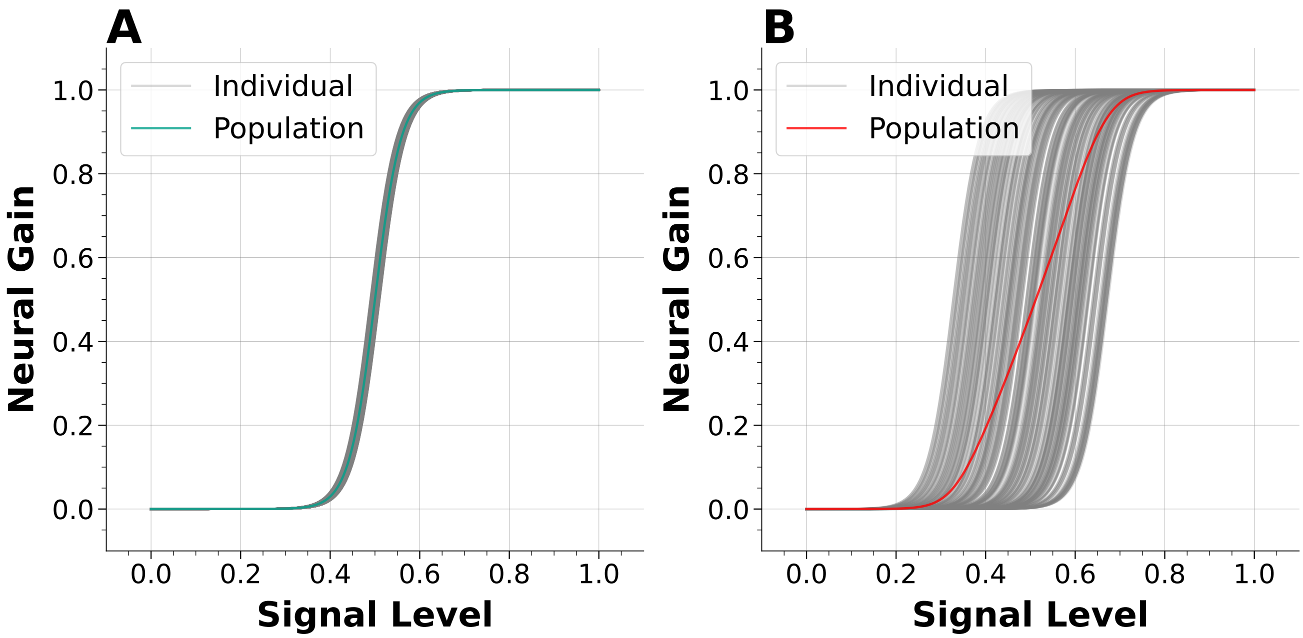

Supplementary Figure 6: Replication of Figure 7 in the main text using the logistic function sigmoid $\frac{1}{\nu + e^{-n(x-k)}}$

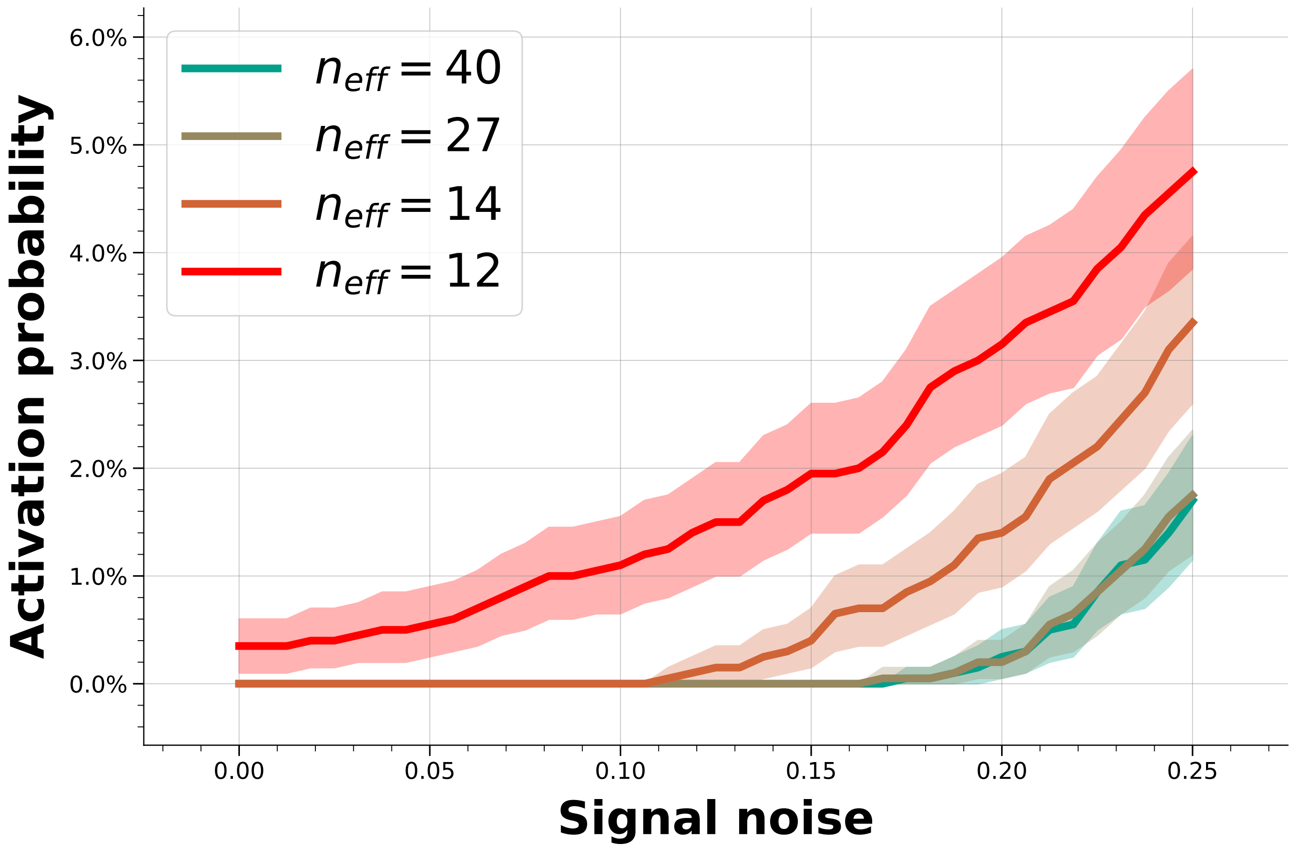

Supplementary Figure 7: Replication of Figure 8 in the main text using the logistic function sigmoid $\frac{1}{\nu + e^{-n(x-k)}}$

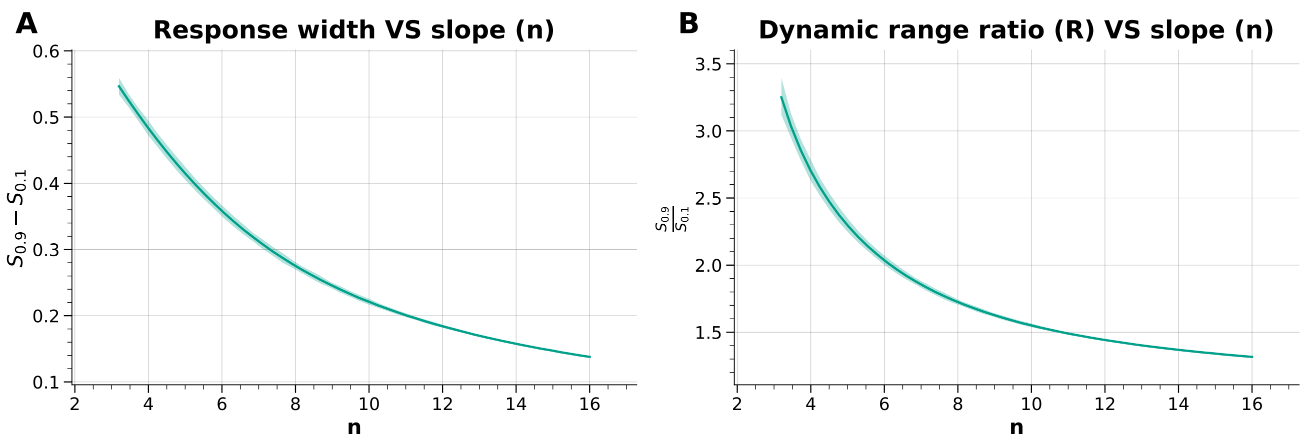

Supplementary Figure 8: **The dynamic range as a function of the slope of the hill equation.** Date are presented as mean±SD.

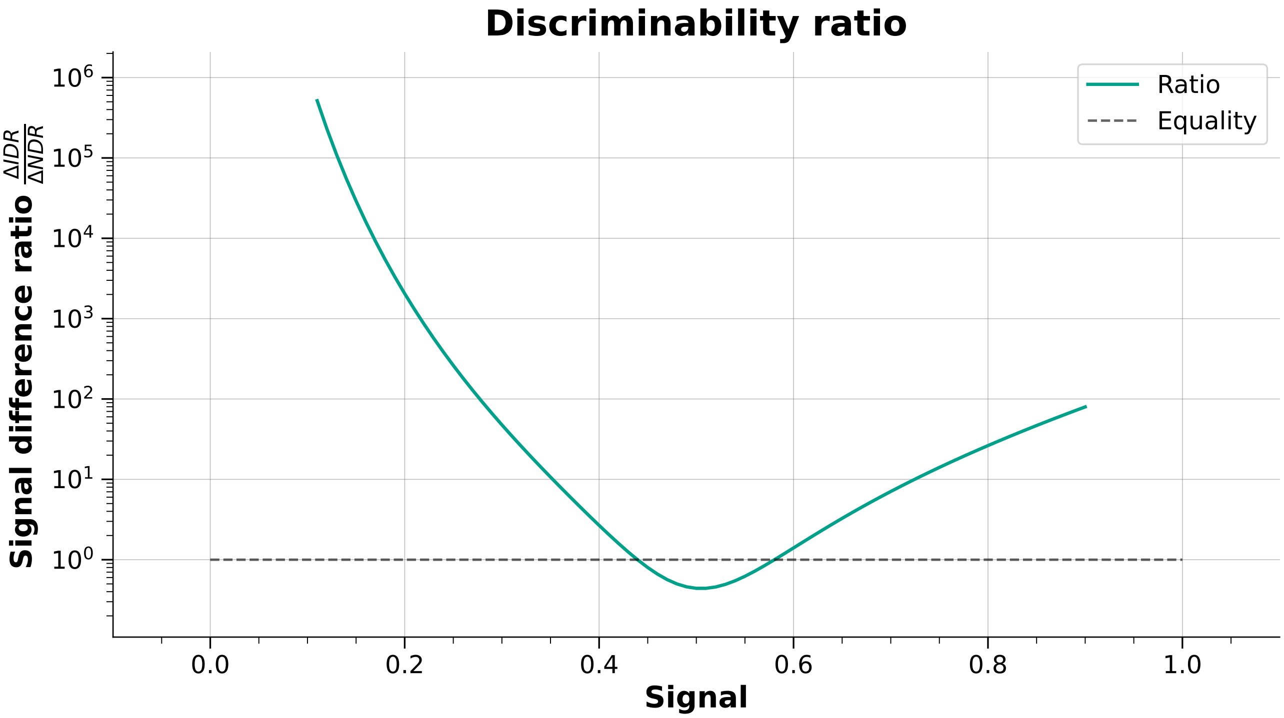

Supplementary Figure 9: **Ratio of increased dynamic range to narrow dynamic range differences between close-by signals.** An increased dynamic range (IDR) response ($n = 7$) and a narrow dynamic range (NDR) response ($n = 16$) were evaluated on the range $[0.1, 0.9]$, with a difference of 0.01 between two close-by signal levels. The difference between close-by signals was evaluated for each pair, and the ratio of IDR to NDR differences was calculated and plotted. IDR shows a discriminability advantage of several orders of magnitude compared with the NDR discriminability for $\tilde{8}0\%$ of the signal range. NDR highest discriminability advantage is only 44% and happens at the center of the input range.

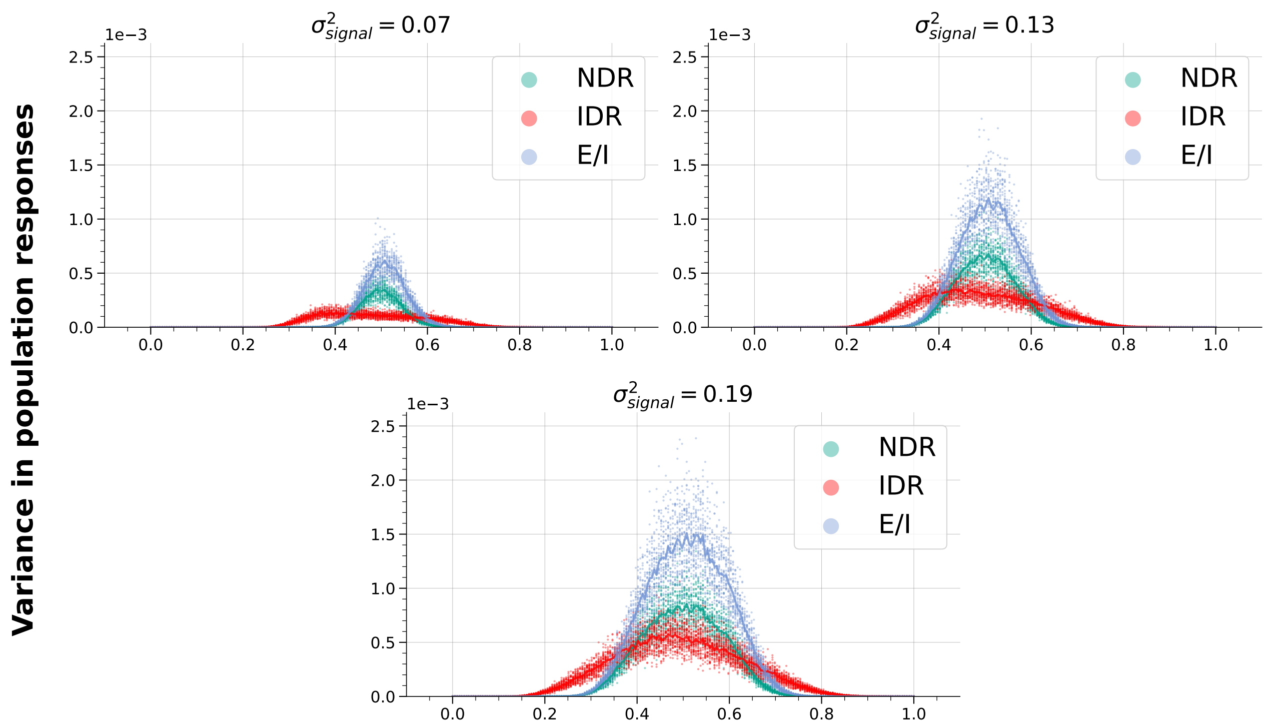

Supplementary Figure 10:
Variance patterns over different levels of noise in the signal. The level of noise in the input signal is indicated by the title of each subplot. The noisier the input signal, the wider are the variance curves in all models.

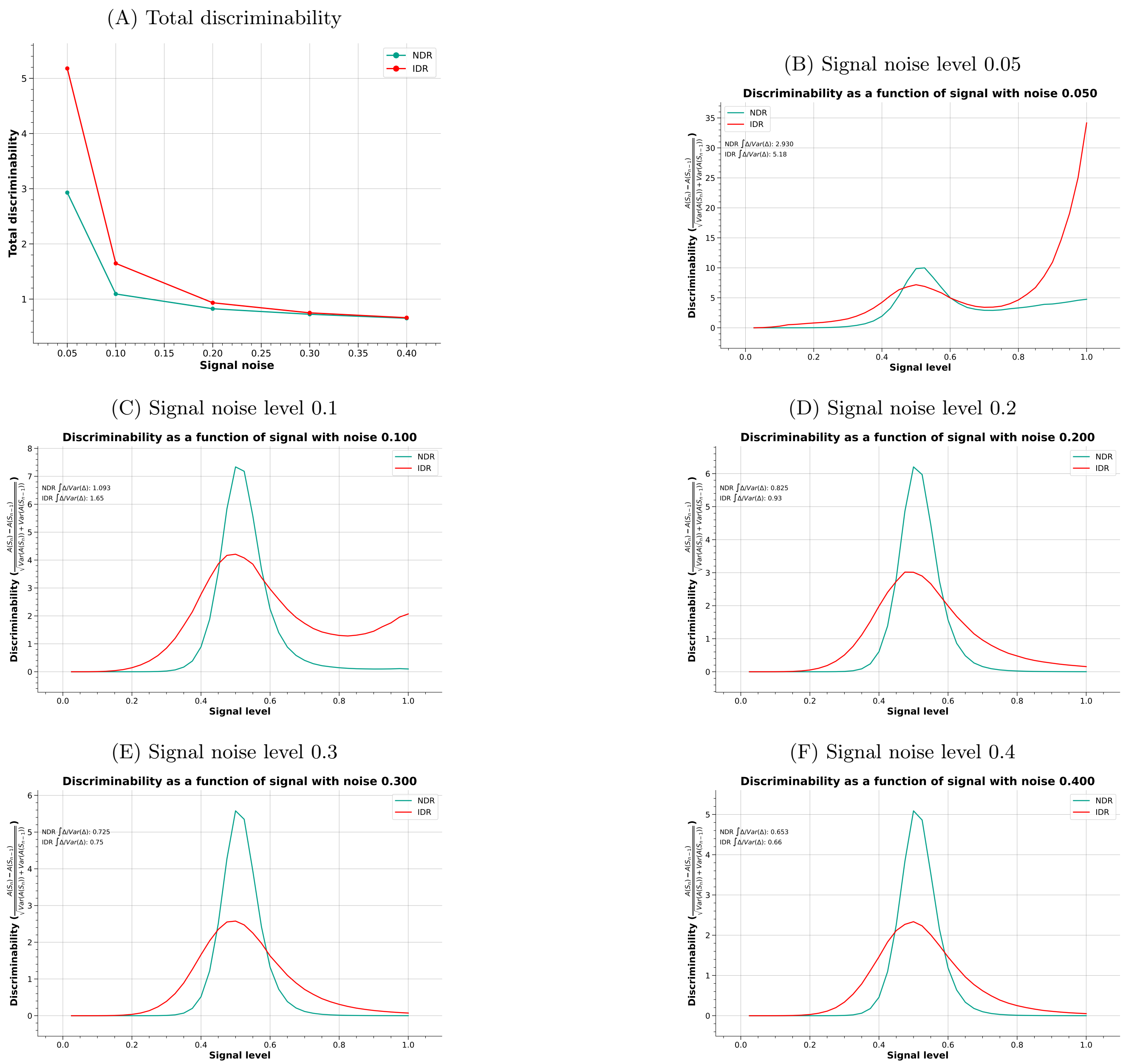

Supplementary Figure 11: **Signal to noise ratio (SNR) for increased dynamic range (IDR) and narrow dynamic range (NDR) across the entire signal range and for different perceptual noise levels.** SNR was calculated in the following manner: $\frac{A_n(S_2)-A_n(S_1)}{\sqrt{Var(A_n(S_1))+Var(A_n(S_2))}}$, where S_1, S_2 are two signal levels sampled from a Gaussian centered around S_1, S_2 respectively (different variances in each subplot), where $S_2 - S_1 = 0.01$. The variances were calculated after applying the Hill equation to 200 samples of the noisy signal $A_n(S_i) = \frac{S^n}{S^n+0.5^n}$. **(A)** Total SNR over the signal range for different noise levels. **(B-F)** SNR curves of increased dynamic range (IDR) and narrow dynamic range (NDR) for different levels of signal noise.

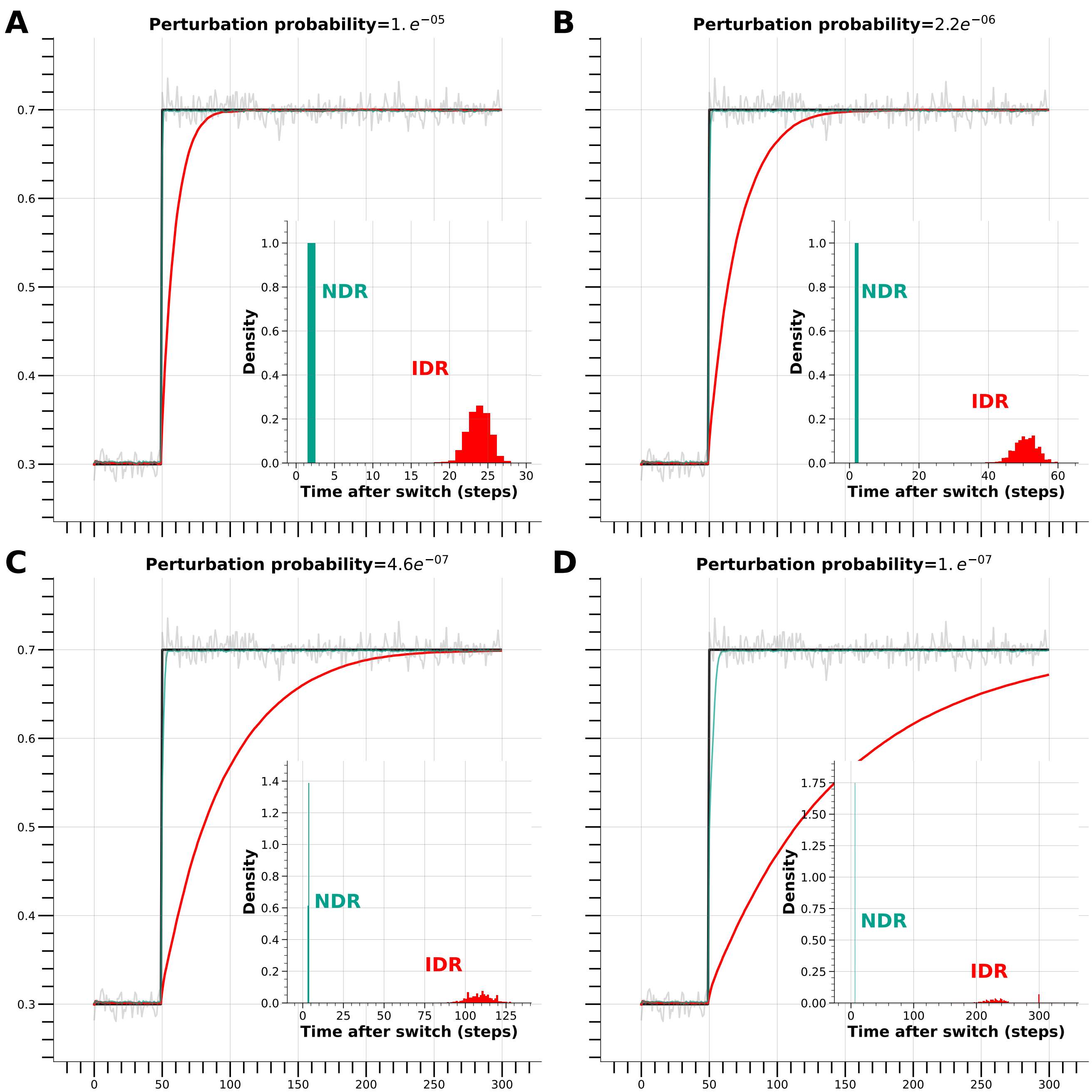

Supplementary Figure 12: **The effect of the perturbation probability on the optimal Bayesian tracking updating rate.** $\sigma^2_{new} = \frac{1}{12}$ for all simulations.

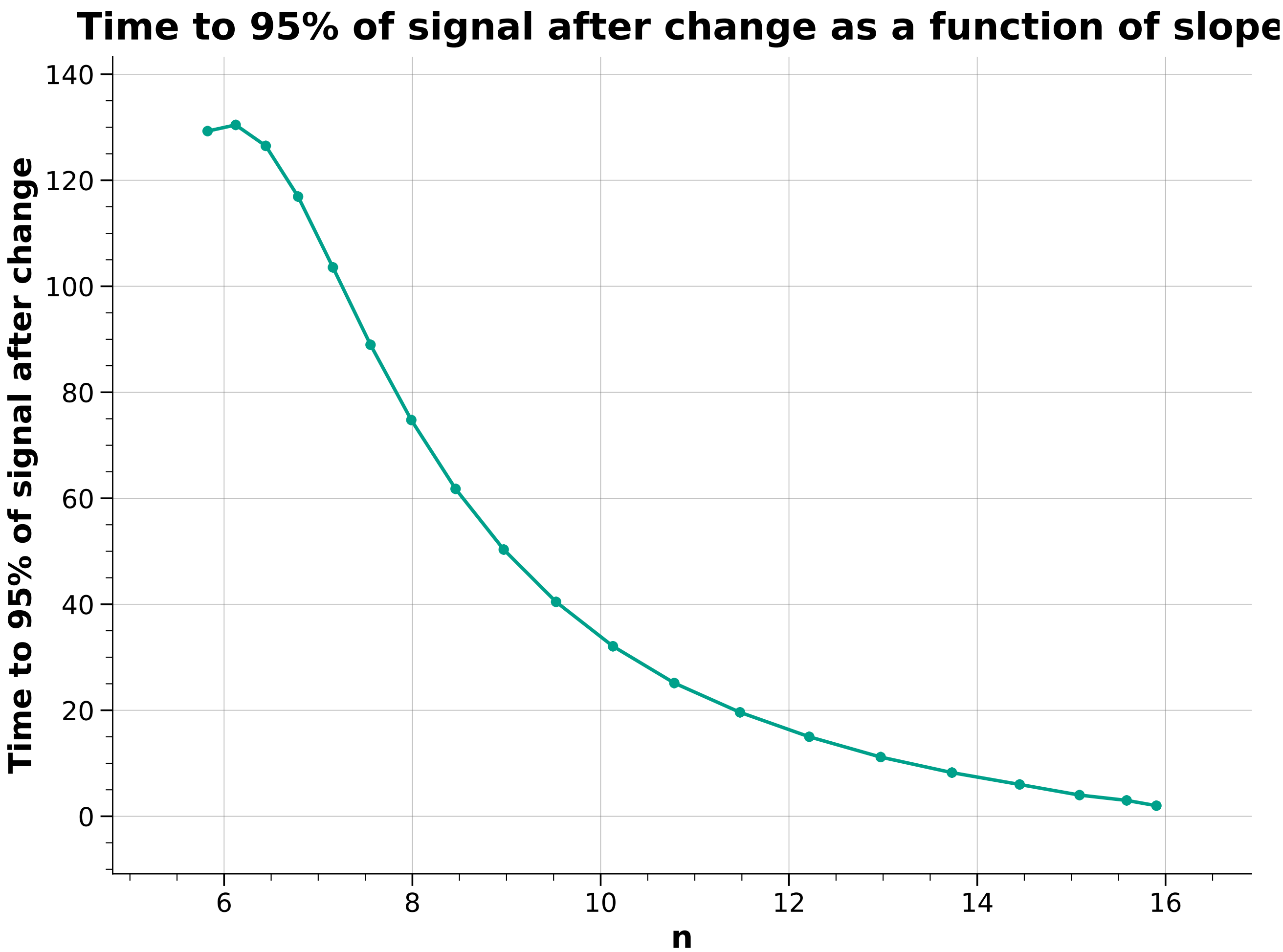

Supplementary Figure 13: Time to track 95% of the signal after an abrupt change as a function of population response function slope.

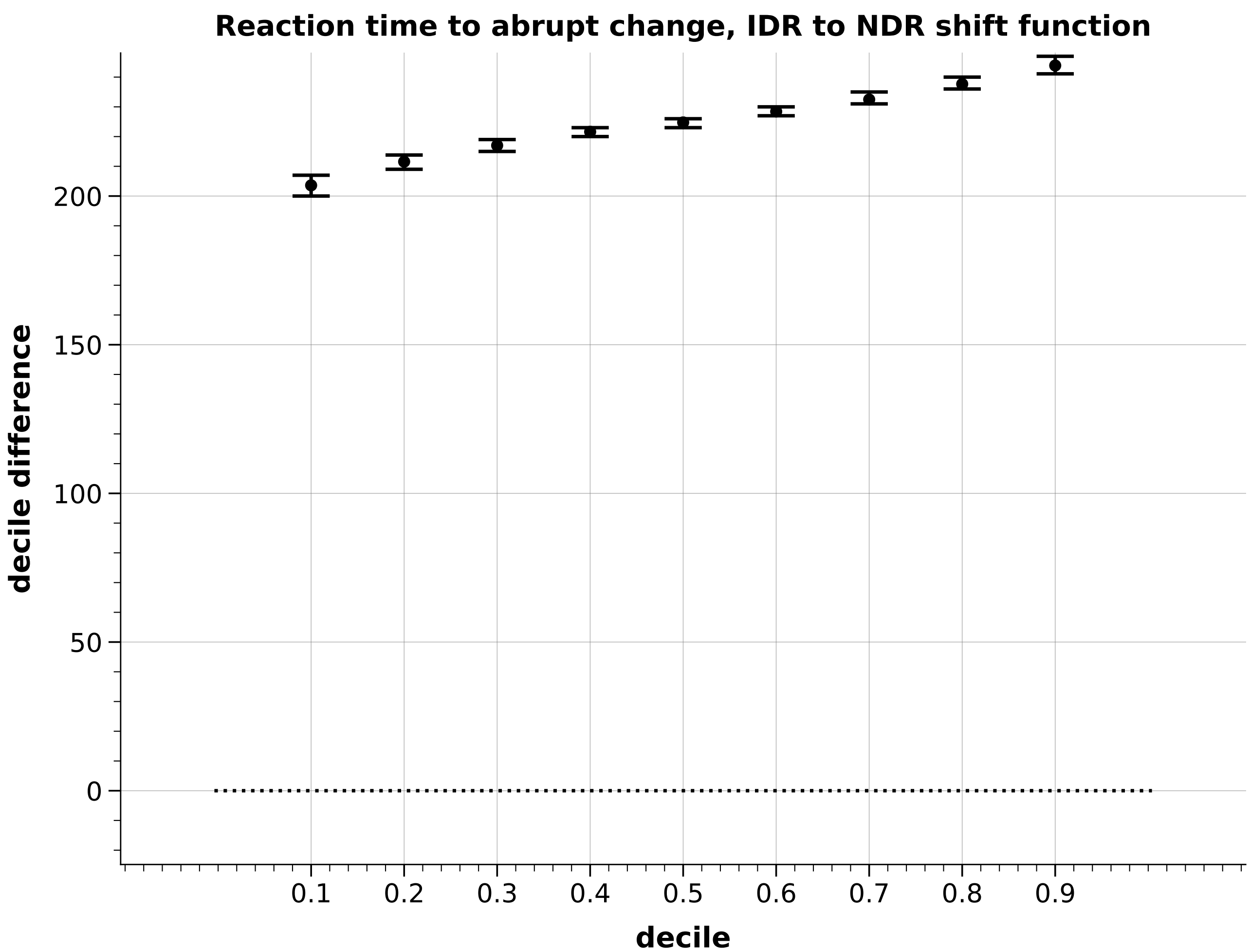

Supplementary Figure 14: **Shift function for increased dynamic range (IDR) - narrow dynamic range (NDR) reaction time to the abrupt change in the input signal.** Comparison of distribution decile difference, black error-bars indicate 95% CI calculated via bootstrapping (10,000 samples).

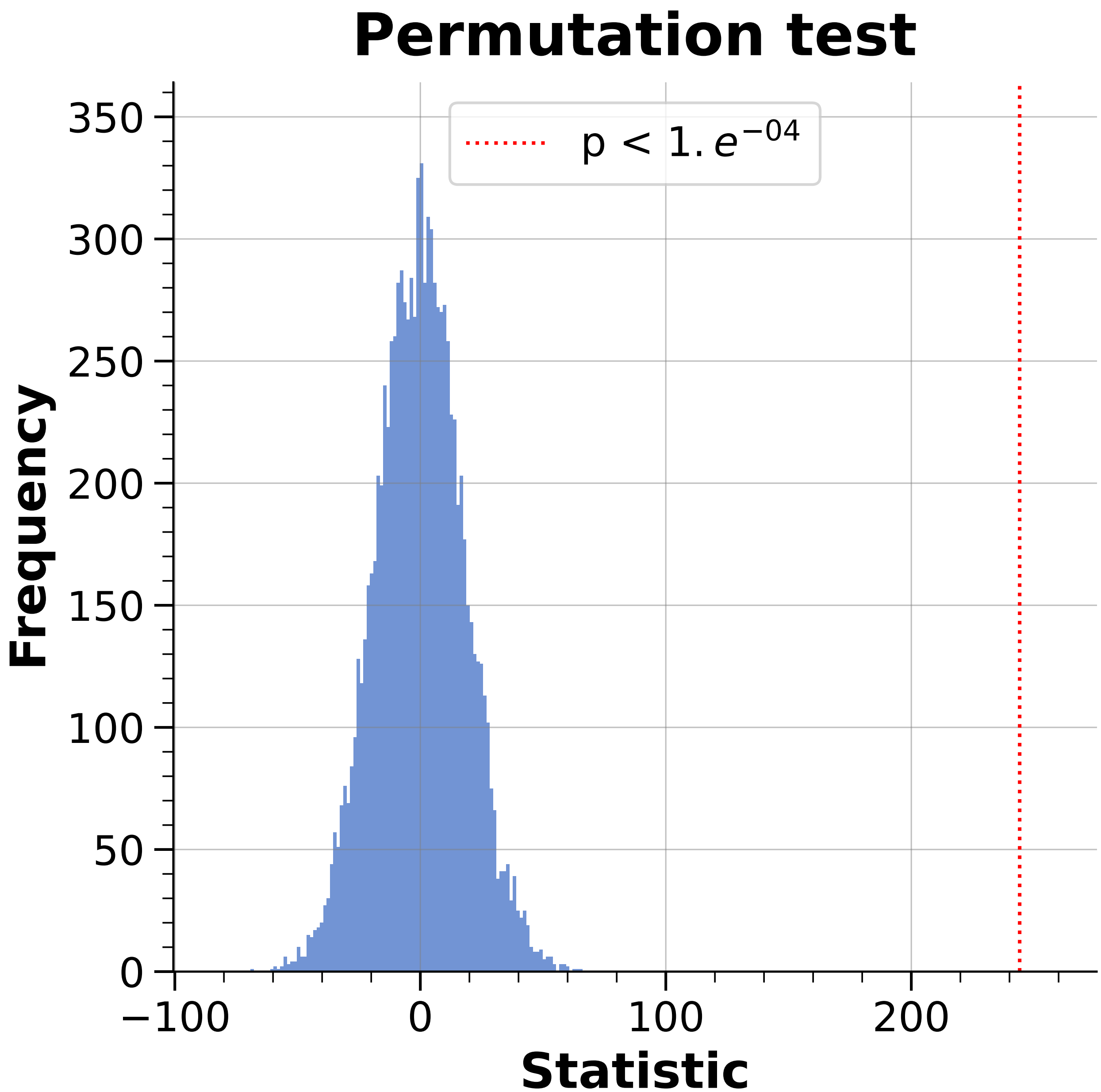

Supplementary Figure 15: **One-sided Permutation test (10,000 permutations) for variance differences, $IDR > NDR$.** Comparison of RT distribution variances, via a permutation test with centering of both distributions before permuting the example labels.

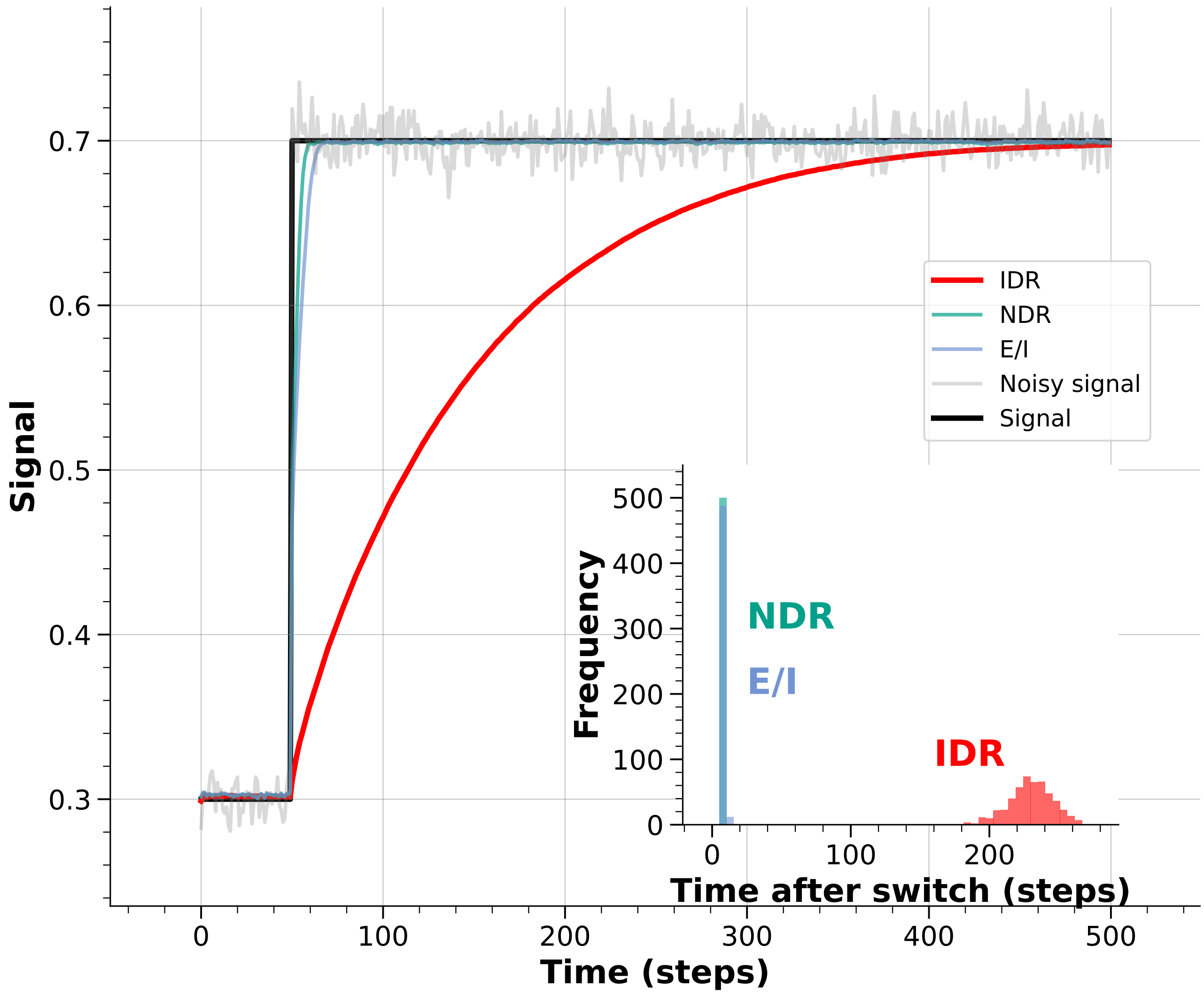

Supplementary Figure 16: **An increased dynamic range entails slower updating to abrupt changes.** A single simulation of tracking an abrupt change in the mean of a noisy signal is plotted, out of 500. The signal had a level of 0.3, with a Gaussian noise of $\mathcal{N}(0.3, 0.01)$, and changed to a level of 0.7 with a Gaussian noise of $\mathcal{N}(0.7, 0.01)$. The black line represents the mean of the signal, while the grey line is a noisy realization of the signal. Optimal Bayesian inference (Kalman filter) was used to estimate the response of a neuronal population to this abrupt signal change. The noisy signal was encoded and then decoded by employing Bayesian inference on three distinct populations - Red, with a gradual population response ($n = 7$), Turquoise, with a sharp population response ($n = 16$), and Light Blue, with a sharp response function and decreased inhibition ($n = 16, \nu = 0.75$). **(Inset)** A histogram of response times to the abrupt change. Response times are the number of time steps needed to reach within 95% of the signal (Response time, mean±std. increased dynamic range (IDR): 229 ± 15.6, narrow dynamic range (NDR): 5 ± 0.2, E/I: 9.5 ± 0.5, one-sided Wilcoxon signed-rank test for $RT_{IDR} > RT_{NDR}$, $W(499) = 0$, $p < 10^{-5}$, $RT_{IDR} > RT_{EI}$, $W(499) = 0$, $p < 10^{-5}$), $RT_{NDR} > RT_{EI}$, $W(499) = 0$, $p < 10^{-5}$.

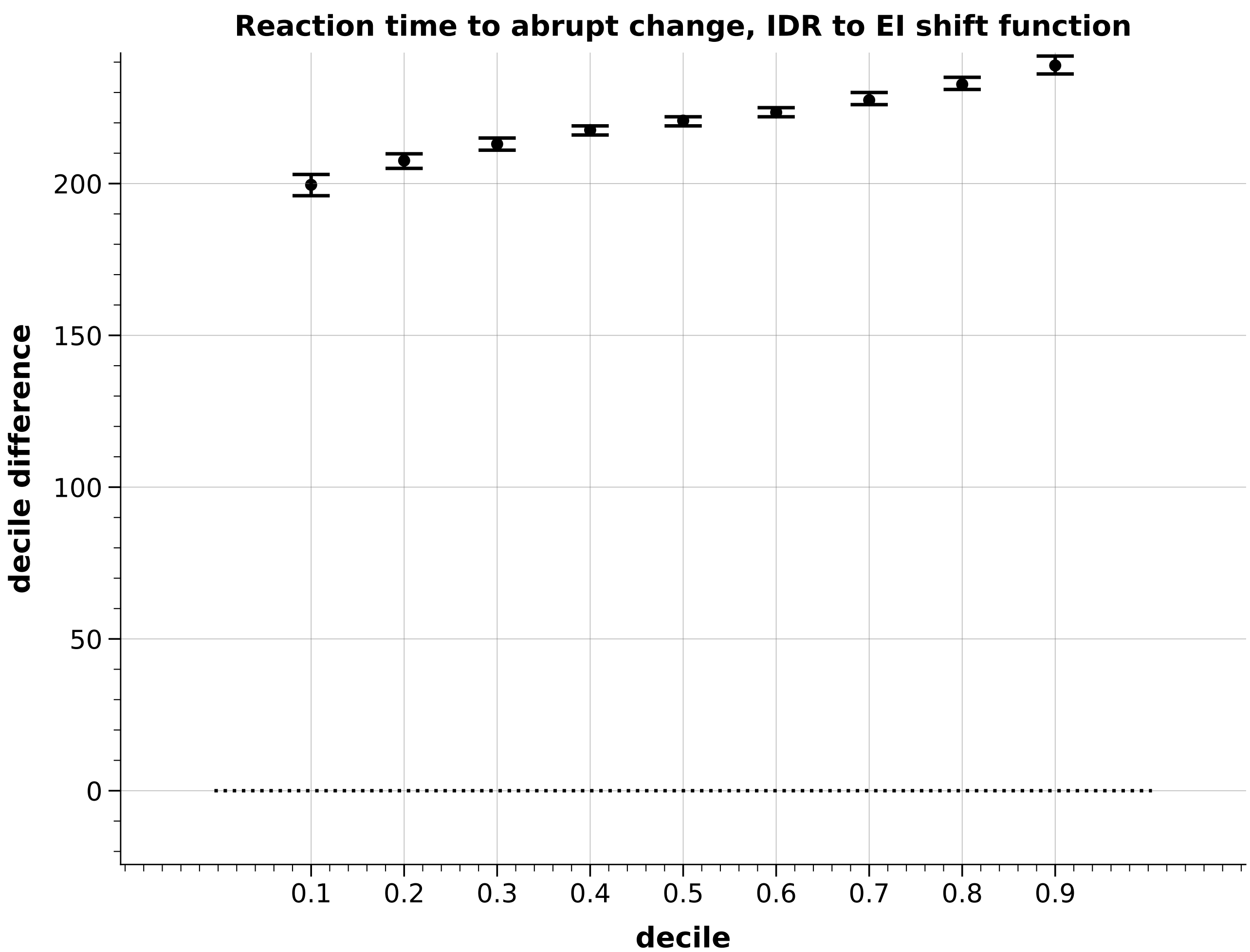

Supplementary Figure 17: **Shift function for increased dynamic range (IDR) - decreased inhibition (EI) reaction time to the abrupt change in the input signal.** Comparison of distribution decile difference, black error-bars indicate 95% CI calculated via bootstrapping (10,000 samples).

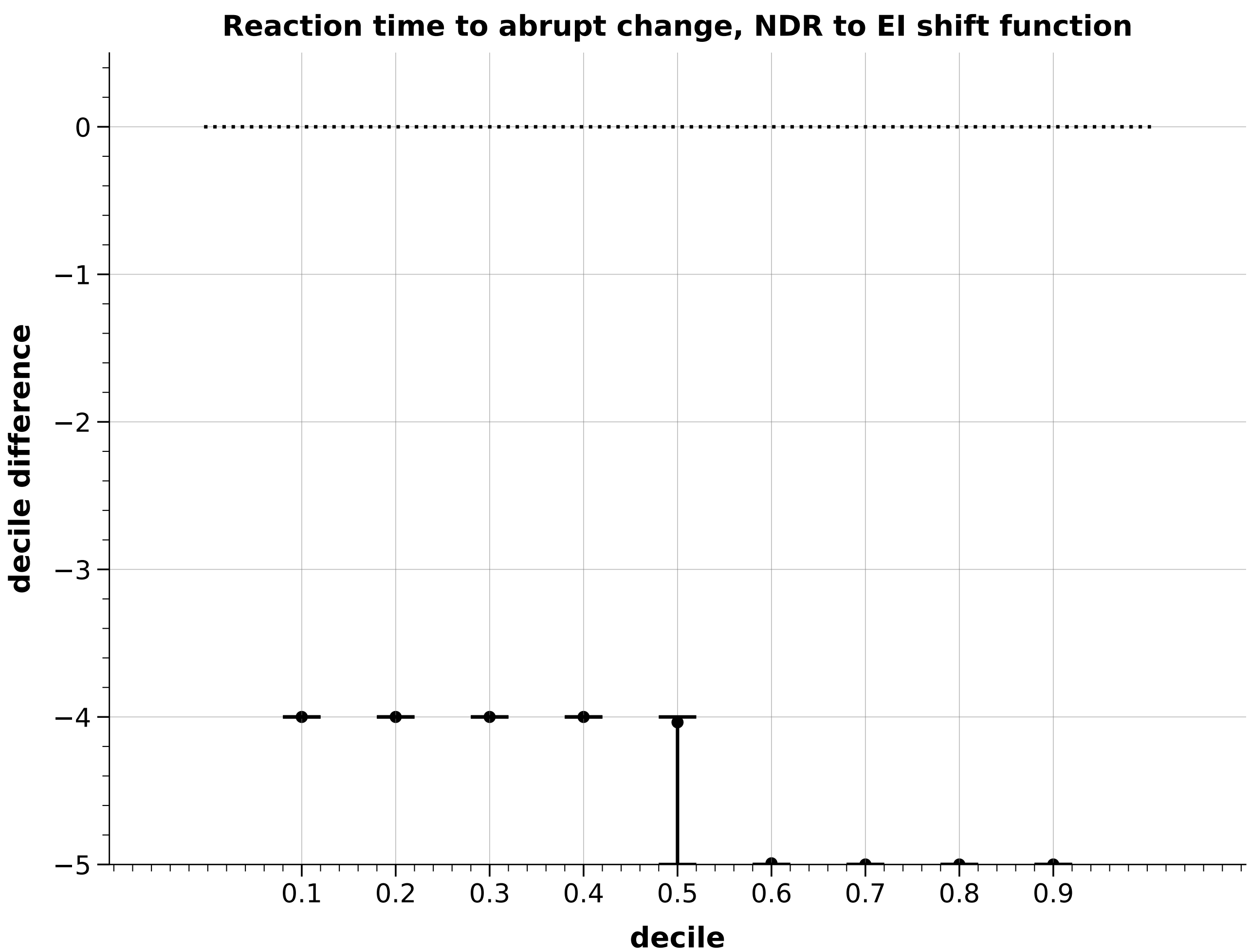

Supplementary Figure 18: **Shift function for narrow dynamic range (NDR) - decreased inhibition (EI) reaction time to the abrupt change in the input signal.** Comparison of distribution decile difference, black error-bars indicate 95% CI calculated via bootstrapping (10,000 samples).

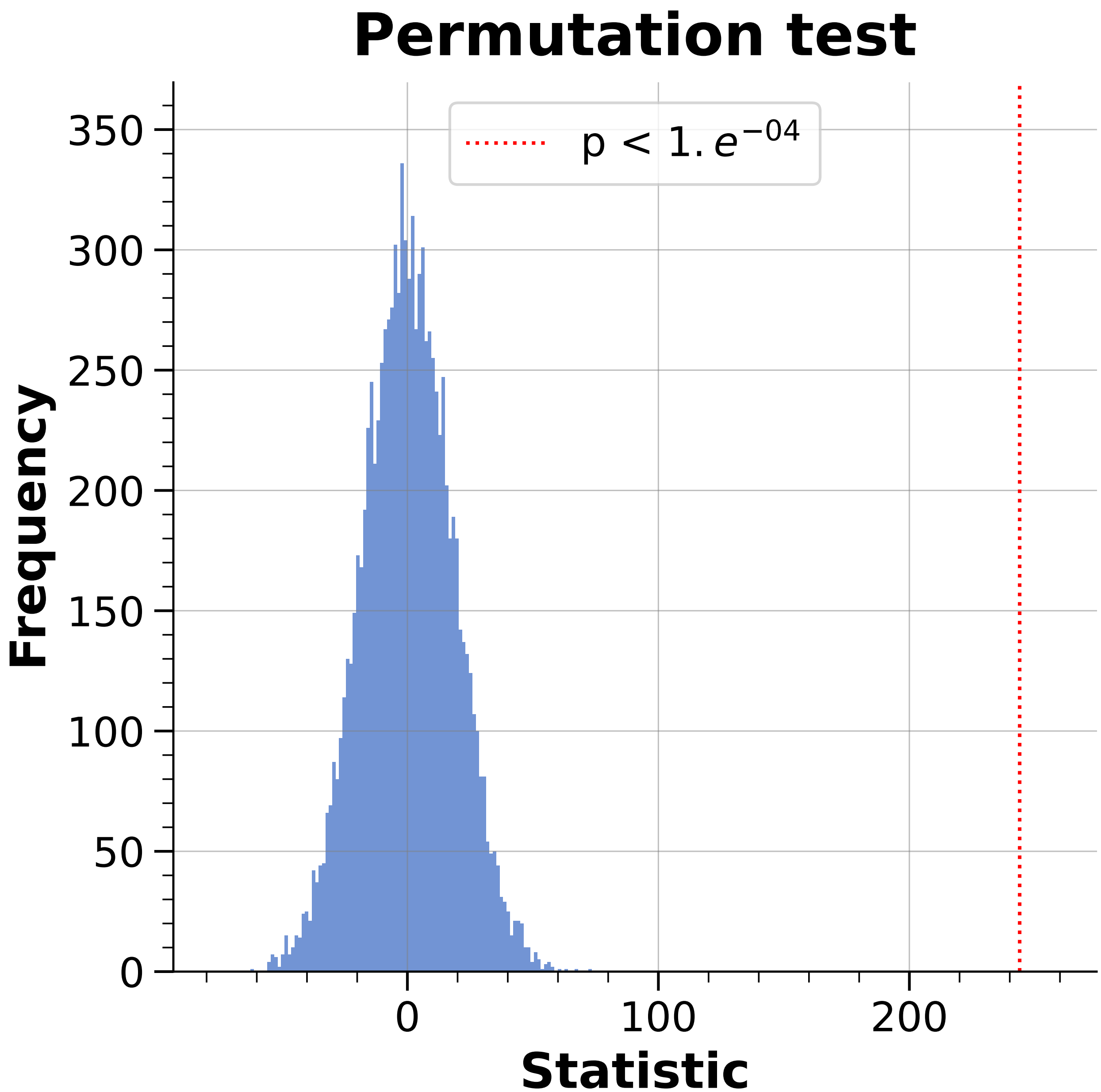

Supplementary Figure 19: **One-sided Permutation test (10,000 permutations) for variance differences, $IDR > EI$.** Comparison of RT distribution variances, via a permutation test with centering of both distributions before permuting the example labels.

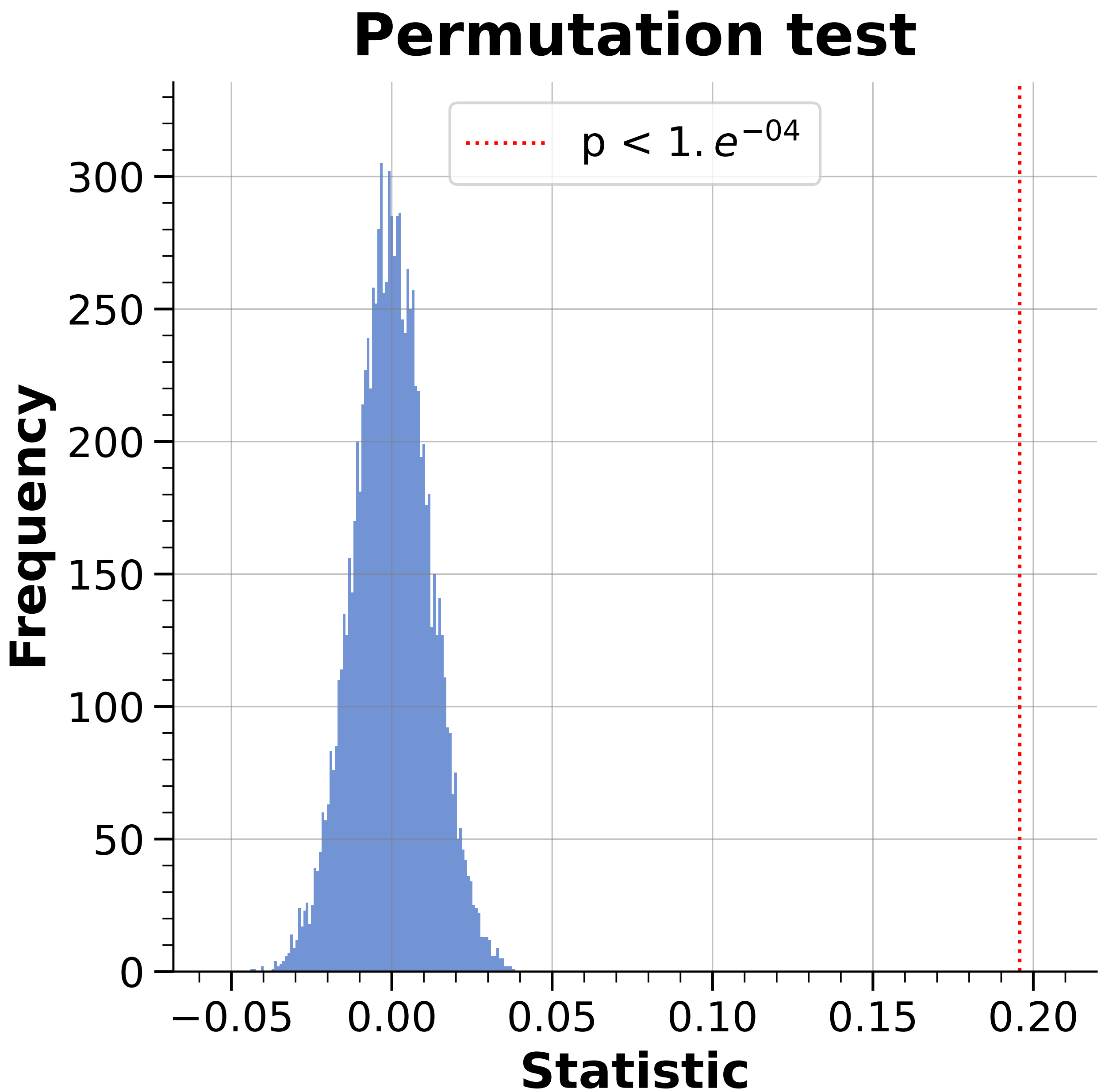

Supplementary Figure 20: **One-sided Permutation test (10,000 permutations) for variance differences, $EI > NDR$.** Comparison of RT distribution variances, via a permutation test with centering of both distributions before permuting the example labels.

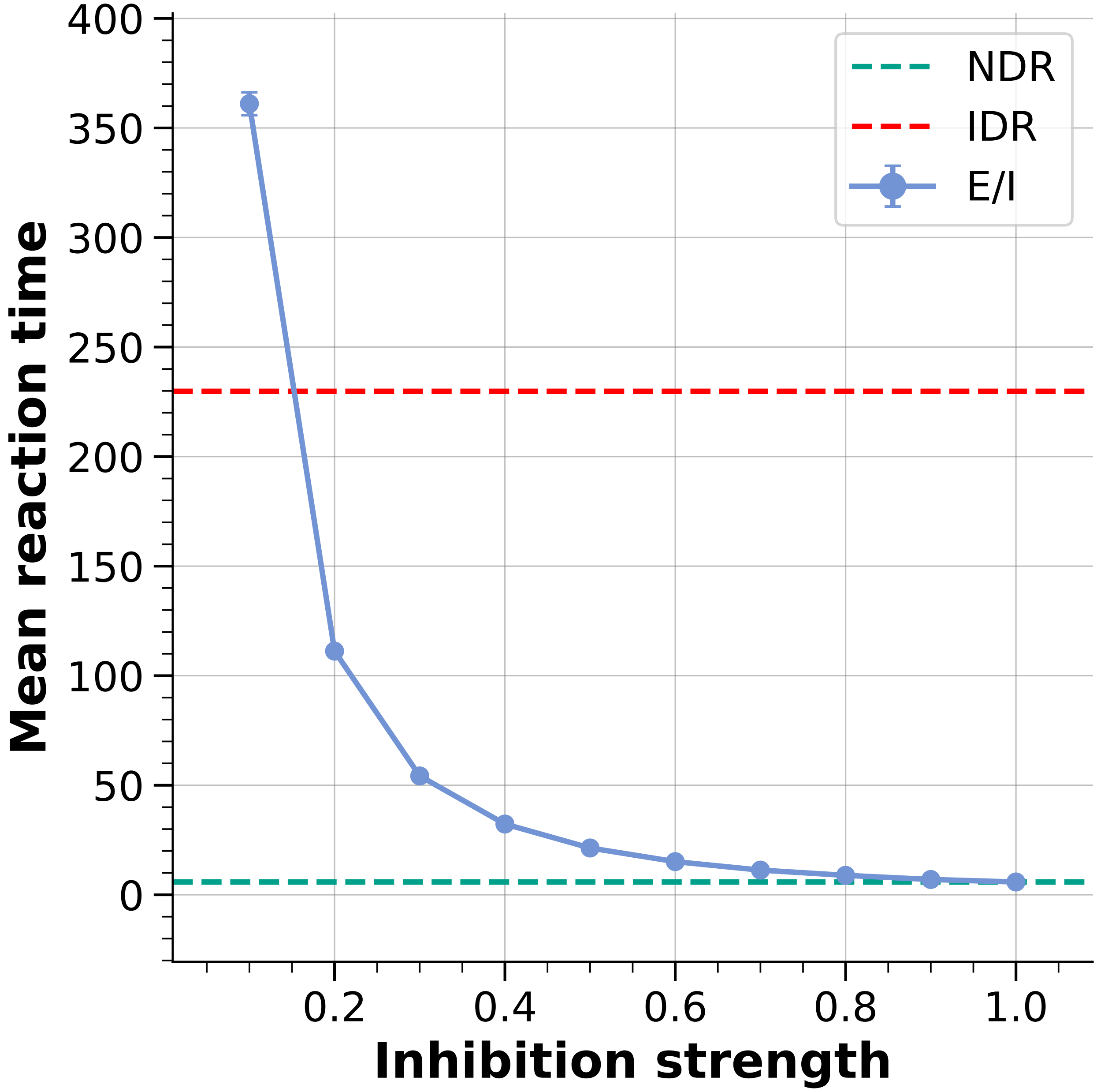

Supplementary Figure 21: **The effect of inhibition strength on the time to track an abrupt signal change. Data points represent mean±SD of 500 simulations, with error bars of ±SD.**

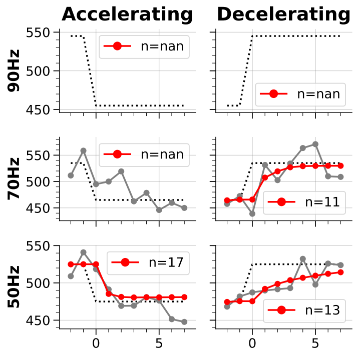

(A) Subject 1

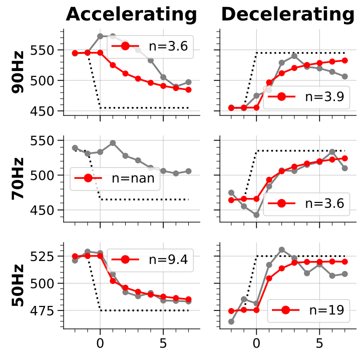

(B) Subject 2

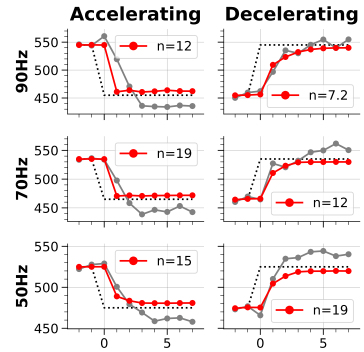

(C) Subject 3

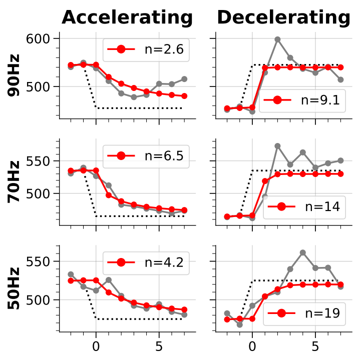

(D) Subject 4

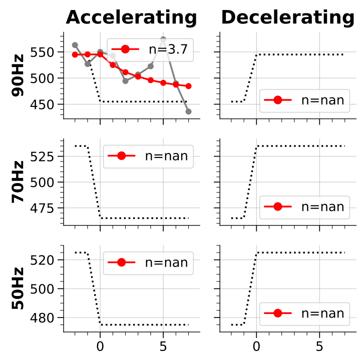

(E) Subject 5

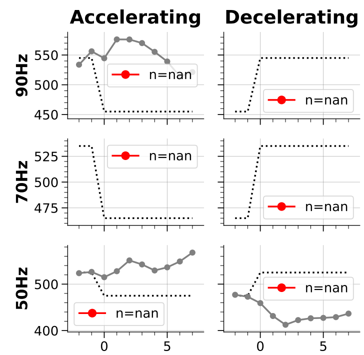

(F) Subject 6

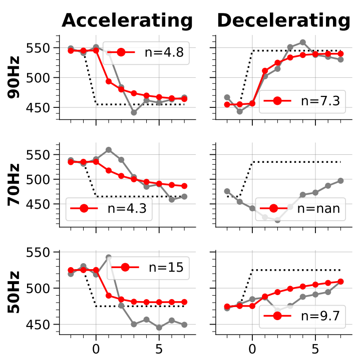

(G) Subject 7

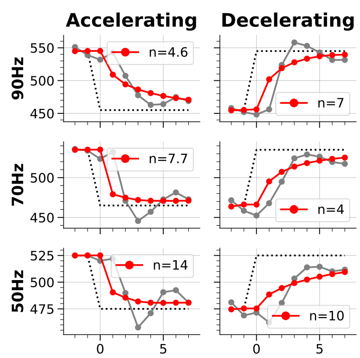

(H) Subject 8

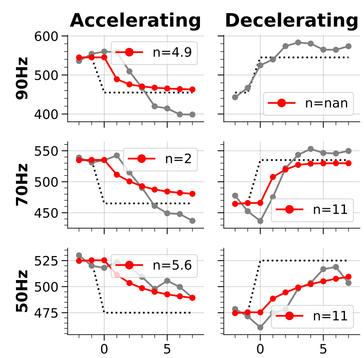

(I) Subject 9

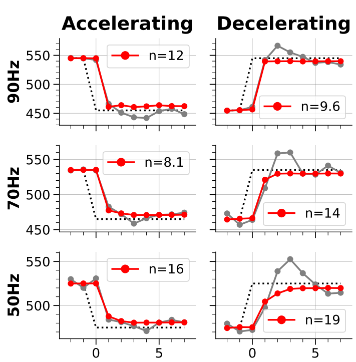

(J) Subject 10

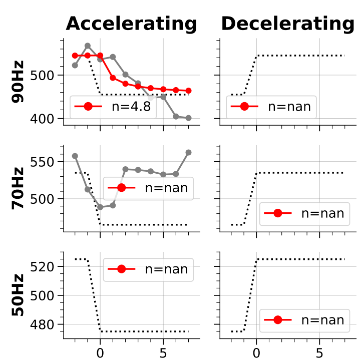

(K) Subject 11

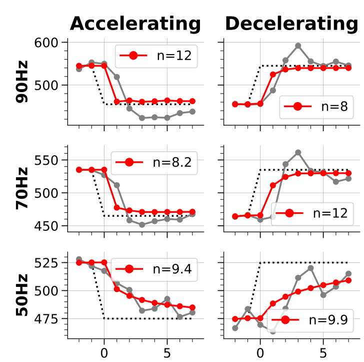

(L) Subject 12

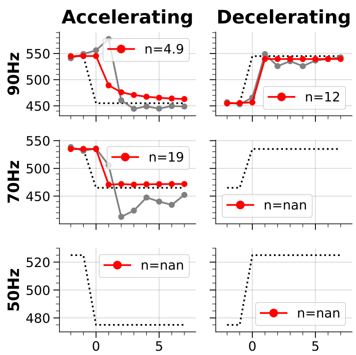

(M) Subject 13

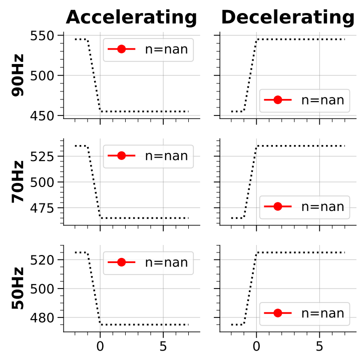

(N) Subject 14

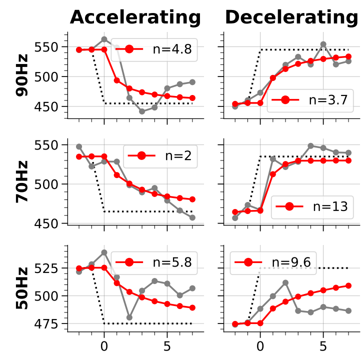

(O) Subject 15

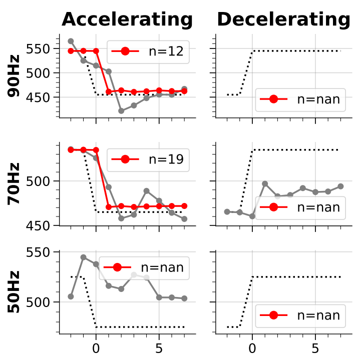

(P) Subject 16

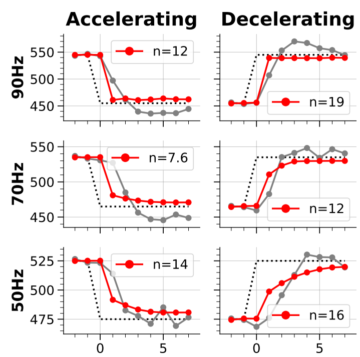

(Q) Subject 17

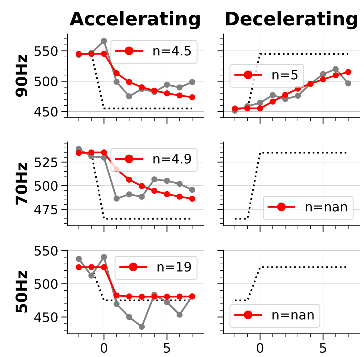

(R) Subject 18

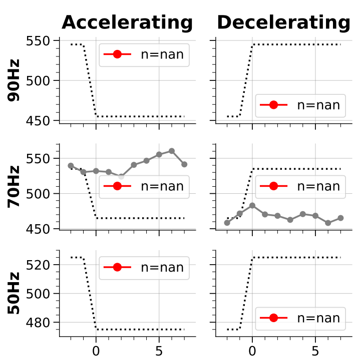

(S) Subject 19

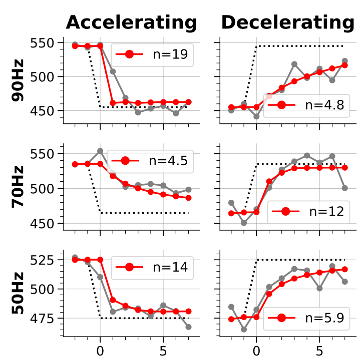

(T) Subject 20

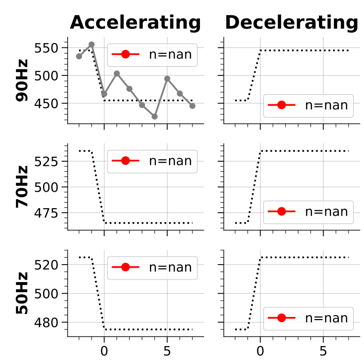

(U) Subject 21

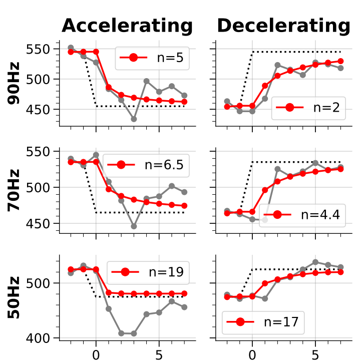

(V) Subject 22

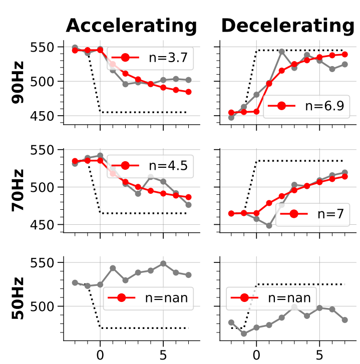

(W) Subject 23

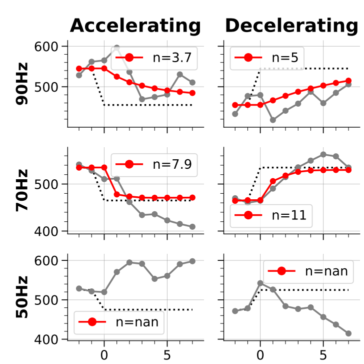

(X) Subject 24

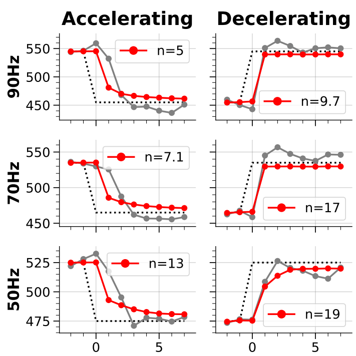

(Y) Subject 25

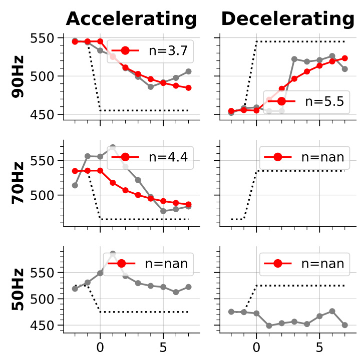

(Z) Subject 26

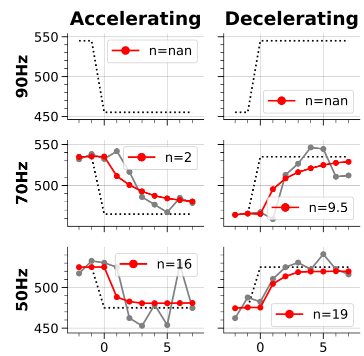

(AA) Subject 27

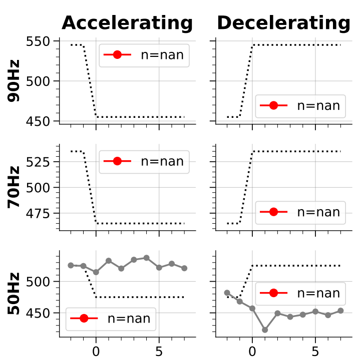

(AB) Subject 28

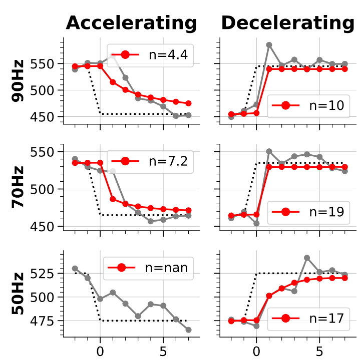

(AC) Subject 29

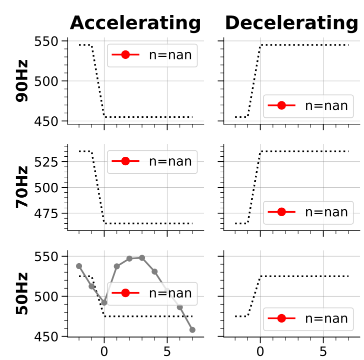

(AD) Subject 30

Supplementary Figure 22: ASD Single subject tapping change dynamics data from Vishne et al.[2] and model fits. Figures without data are subjects who did not have 3 or more occurrences of the specific frequency change without missed responses. Figures with data but without model fits are change dynamics that do not track the change and were thus not fitted.

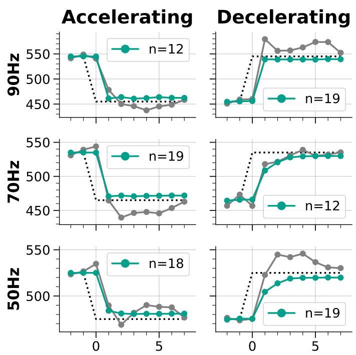

(A) Subject 1

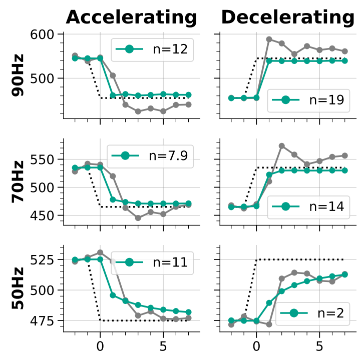

(B) Subject 2

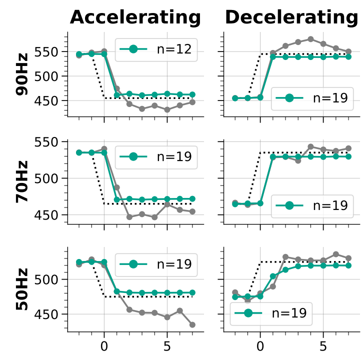

(C) Subject 3

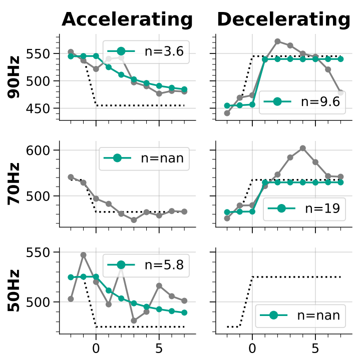

(D) Subject 4

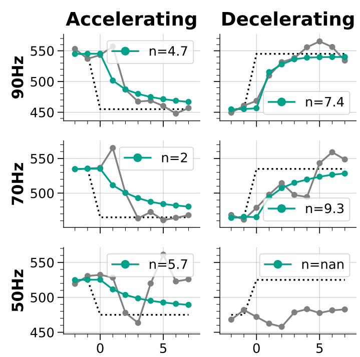

(E) Subject 5

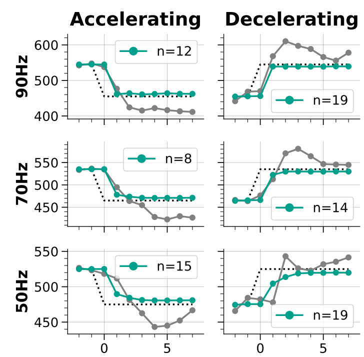

(F) Subject 6

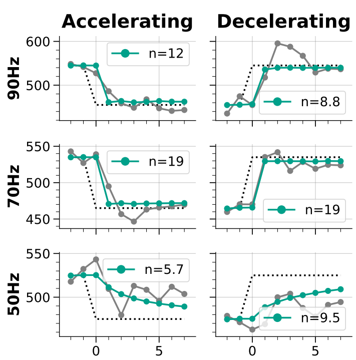

(G) Subject 7

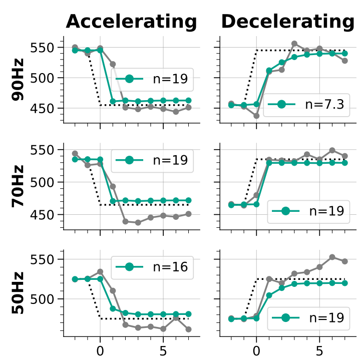

(H) Subject 8

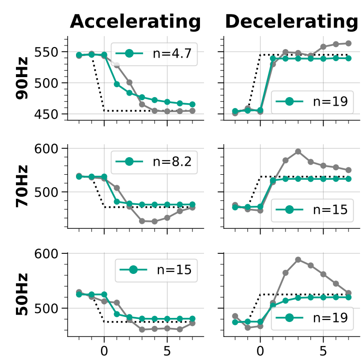

(I) Subject 9

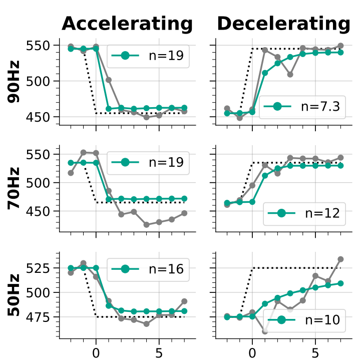

(J) Subject 10

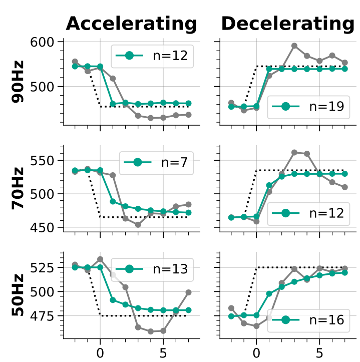

(K) Subject 11

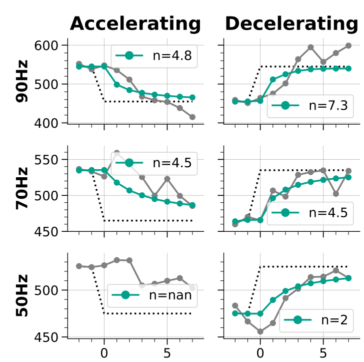

(L) Subject 12

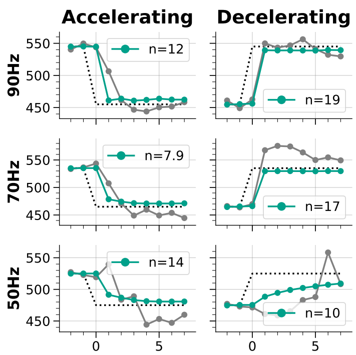

(M) Subject 13

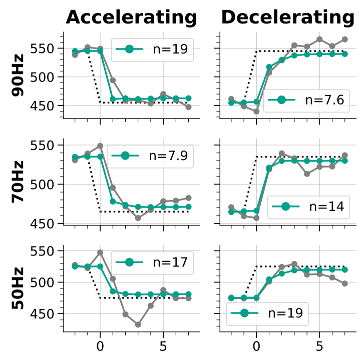

(N) Subject 14

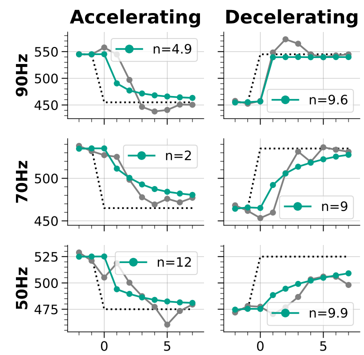

(O) Subject 15

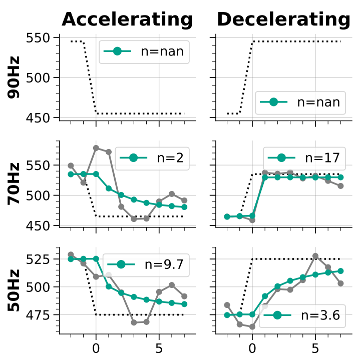

(P) Subject 16

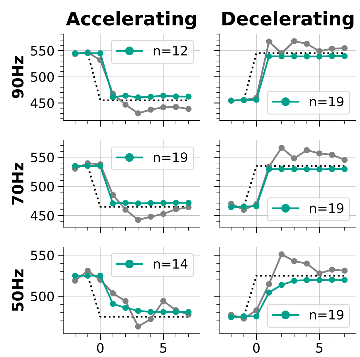

(Q) Subject 17

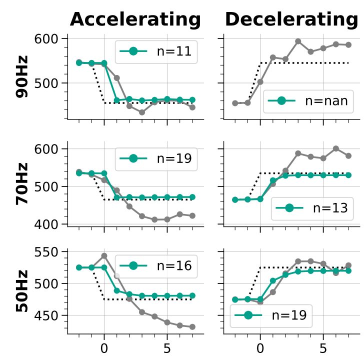

(R) Subject 18

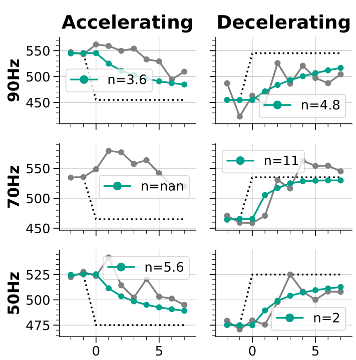

(S) Subject 19

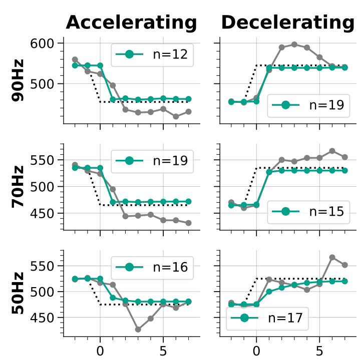

(T) Subject 20

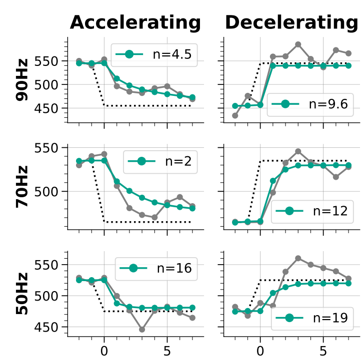

(U) Subject 21

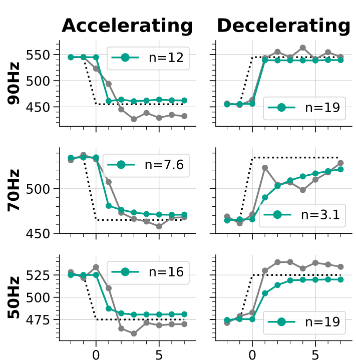

(V) Subject 22

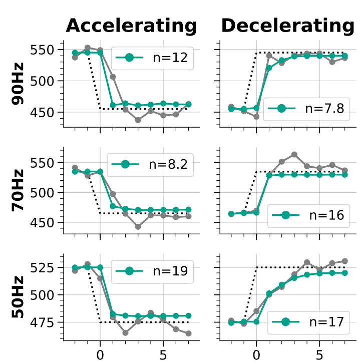

(W) Subject 23

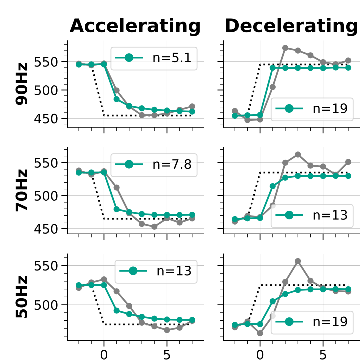

(X) Subject 24

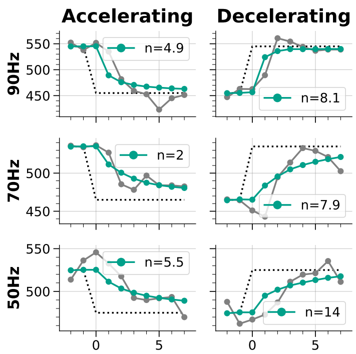

(Y) Subject 25

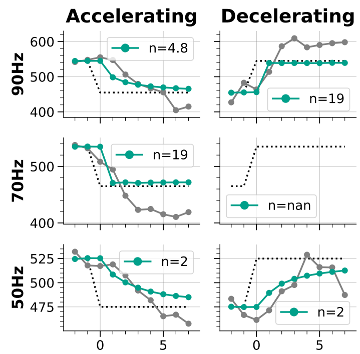

(Z) Subject 26

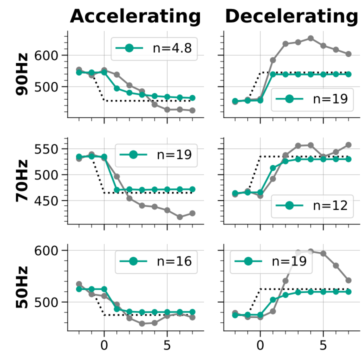

(AA) Subject 27

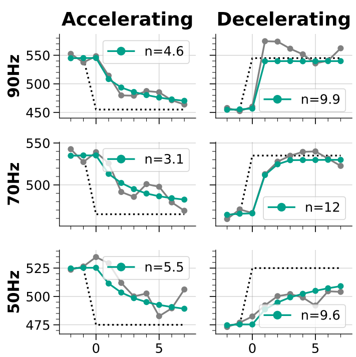

(AB) Subject 28

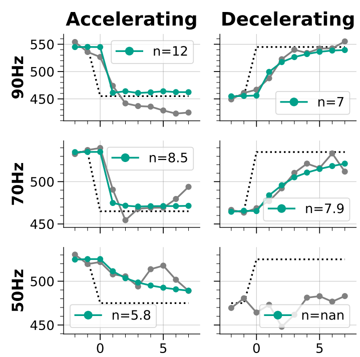

(AC) Subject 29

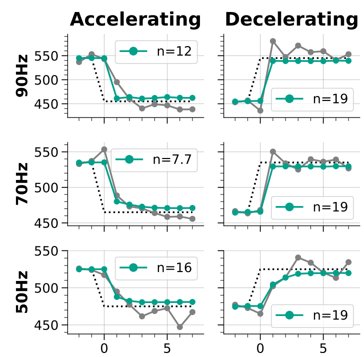

(AD) Subject 30

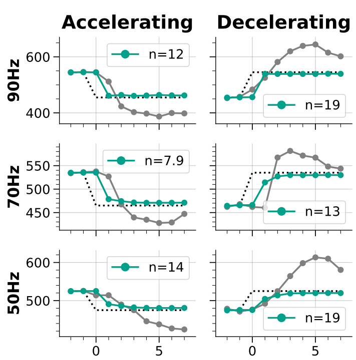

(AE) Subject 31

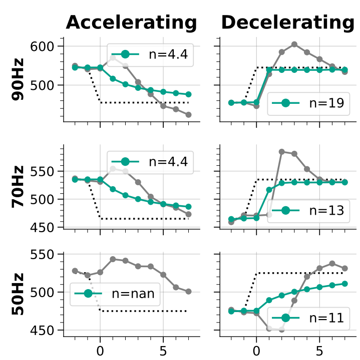

(AF) Subject 32

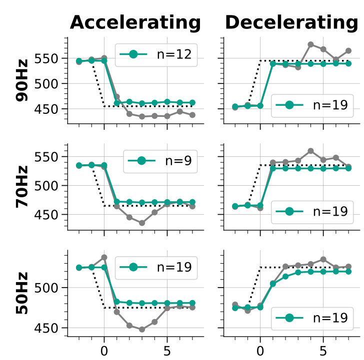

(AG) Subject 33

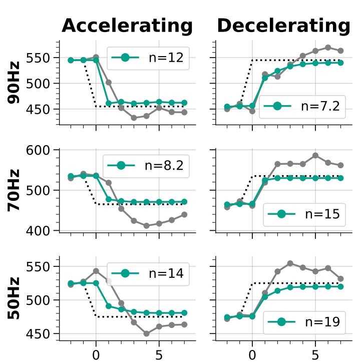

(AH) Subject 34

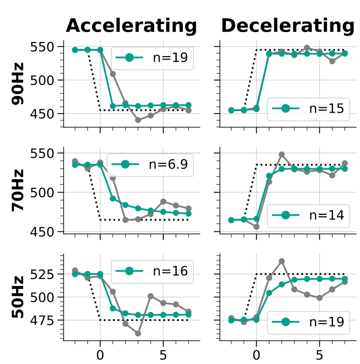

(AI) Subject 35

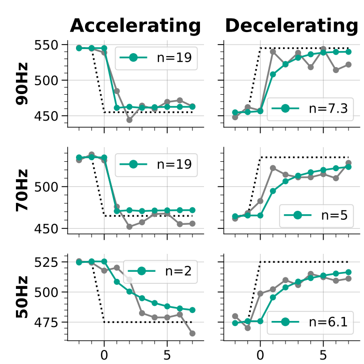

(AJ) Subject 36

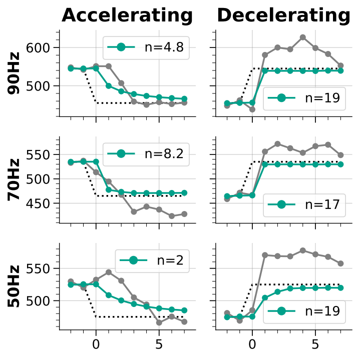

(AK) Subject 37

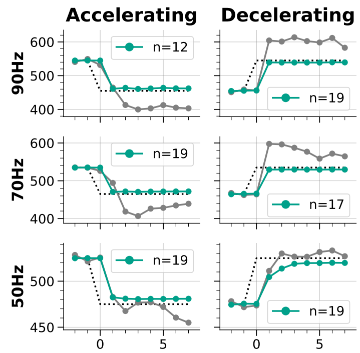

(AL) Subject 38

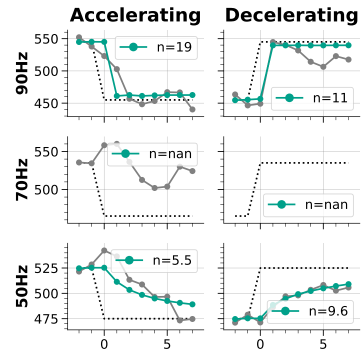

(AM) Subject 39

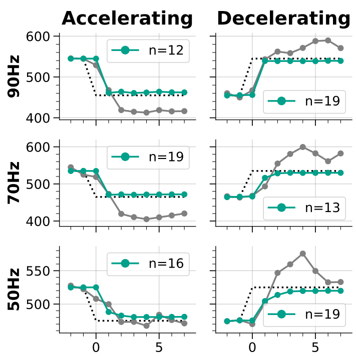

(AN) Subject 40

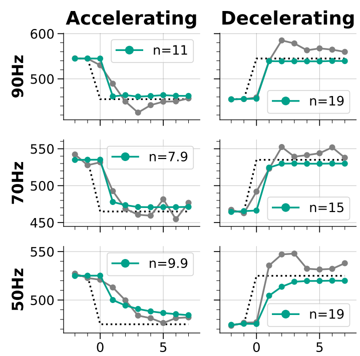

(AO) Subject 41

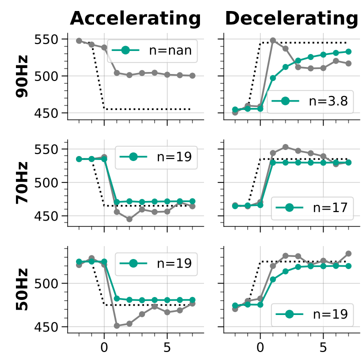

(AP) Subject 42

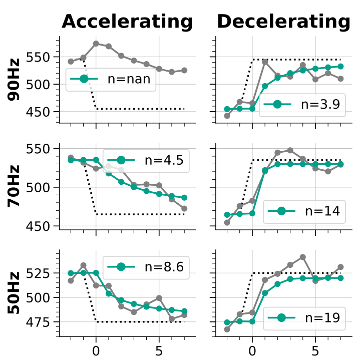

(AQ) Subject 43

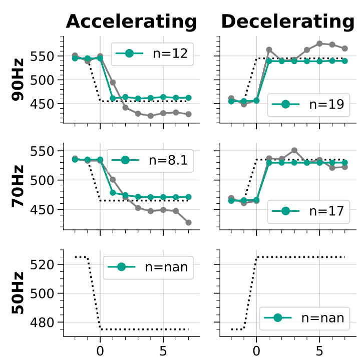

(AR) Subject 44

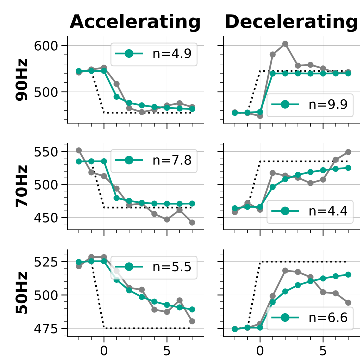

(AS) Subject 45

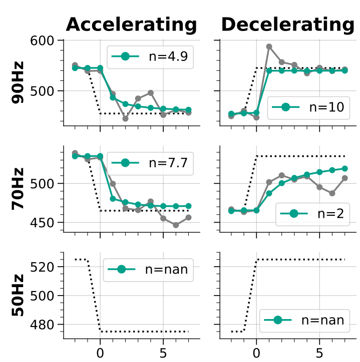

(AT) Subject 46

Supplementary Figure 23: NT Single subject tapping change dynamics data from Vishne et al.[2] and model fits. Figures without data are subjects who did not have 3 or more occurrences of the specific frequency change without missed responses. Figures with data but without model fits are change dynamics that do not track the change and were thus not fitted.

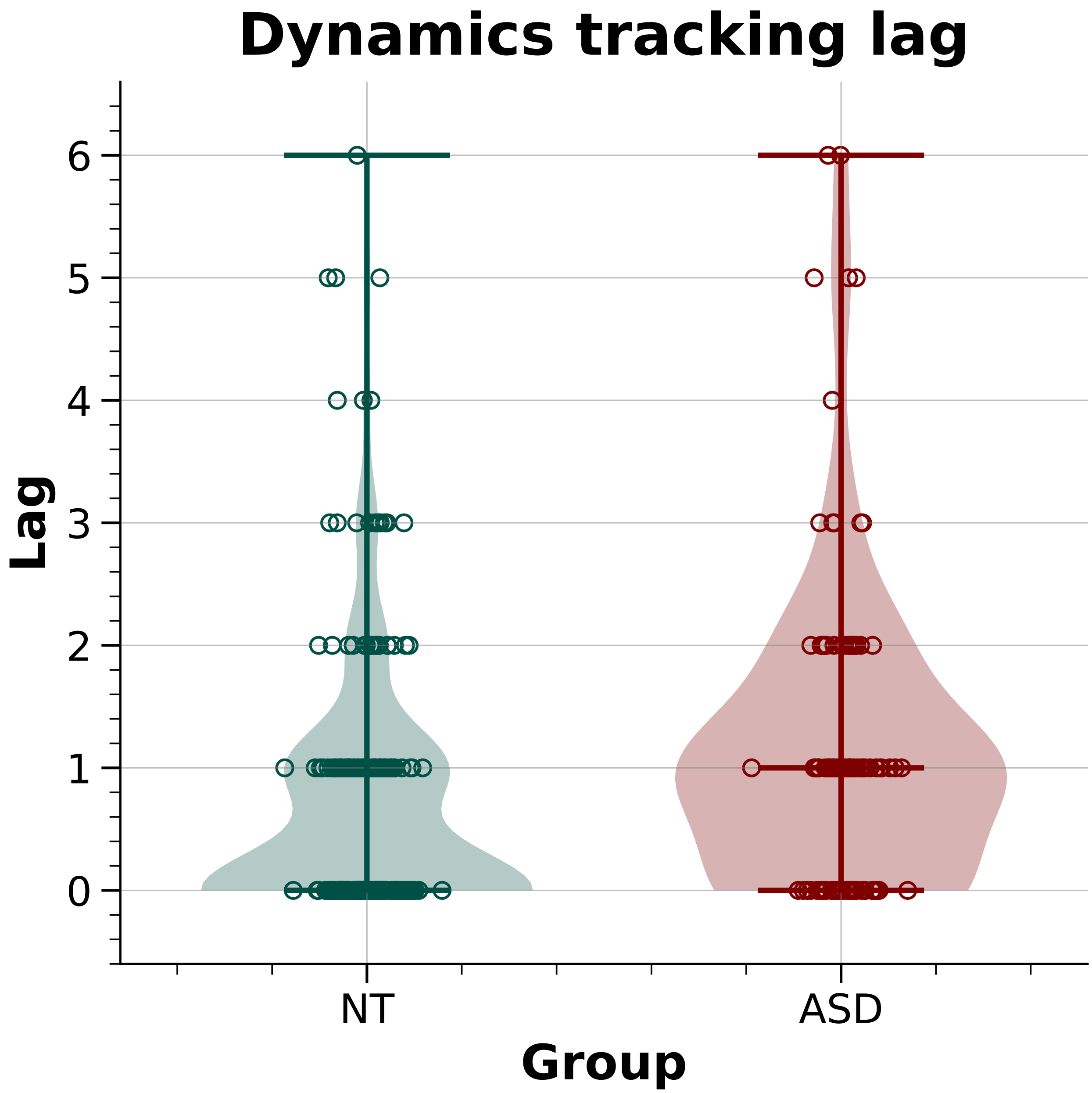

Supplementary Figure 24: **Distribution of tracking times per subject in Vishne et al.[2].** Tracking time was defined as the number of steps after the perceived change in metronome frequency in which the average change dynamics passed 500Hz.

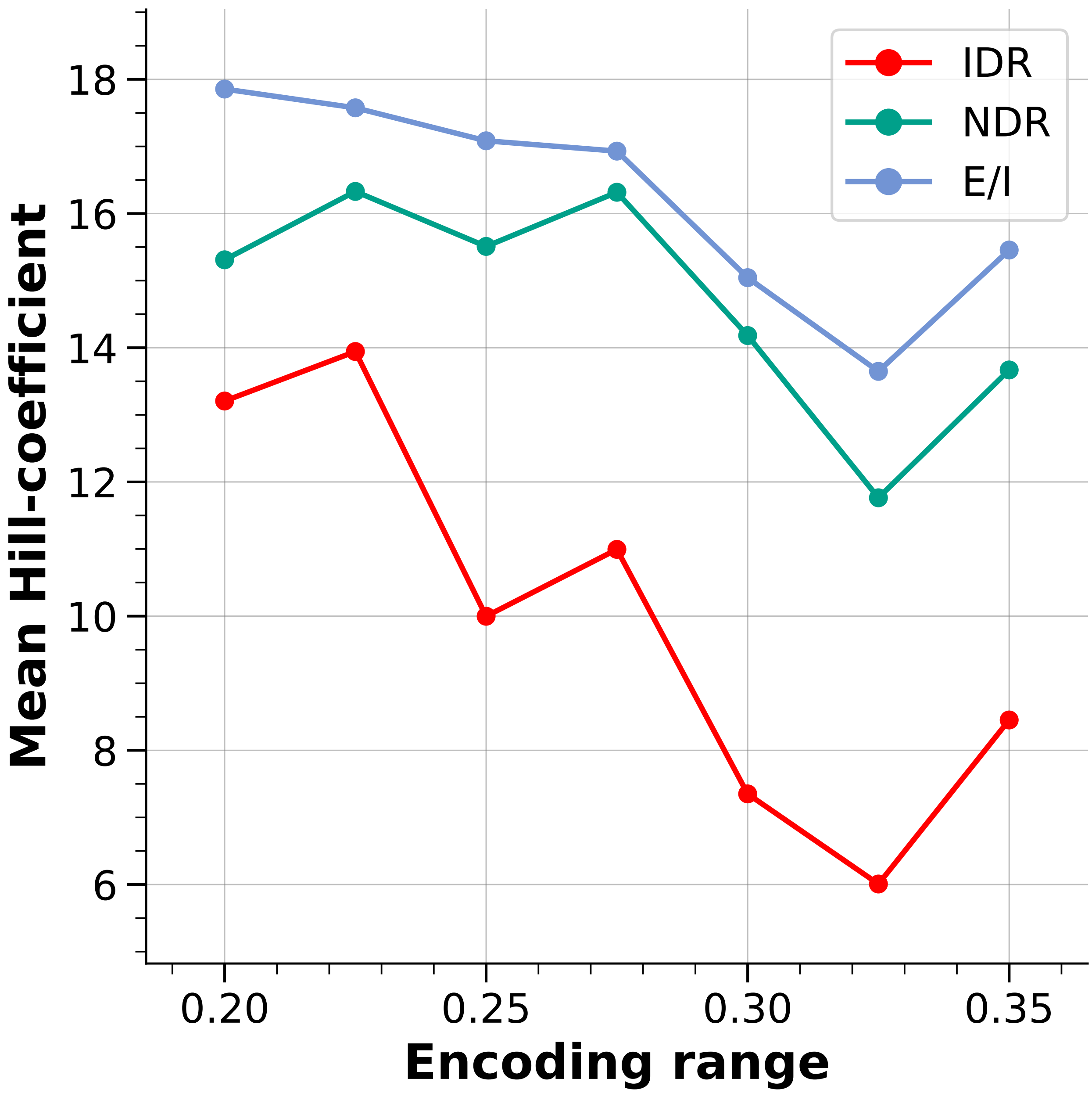

Supplementary Figure 25: **Sensitivity of the fitting procedure to the encoding range.** Mean Hill-coefficients of group-level fits to the tapping data for different ranges of encoding. An encoding range of 0.2 around 0.5 means that metronome frequencies of [455, 545] are mapped to input signals of [0.3, 0.7].

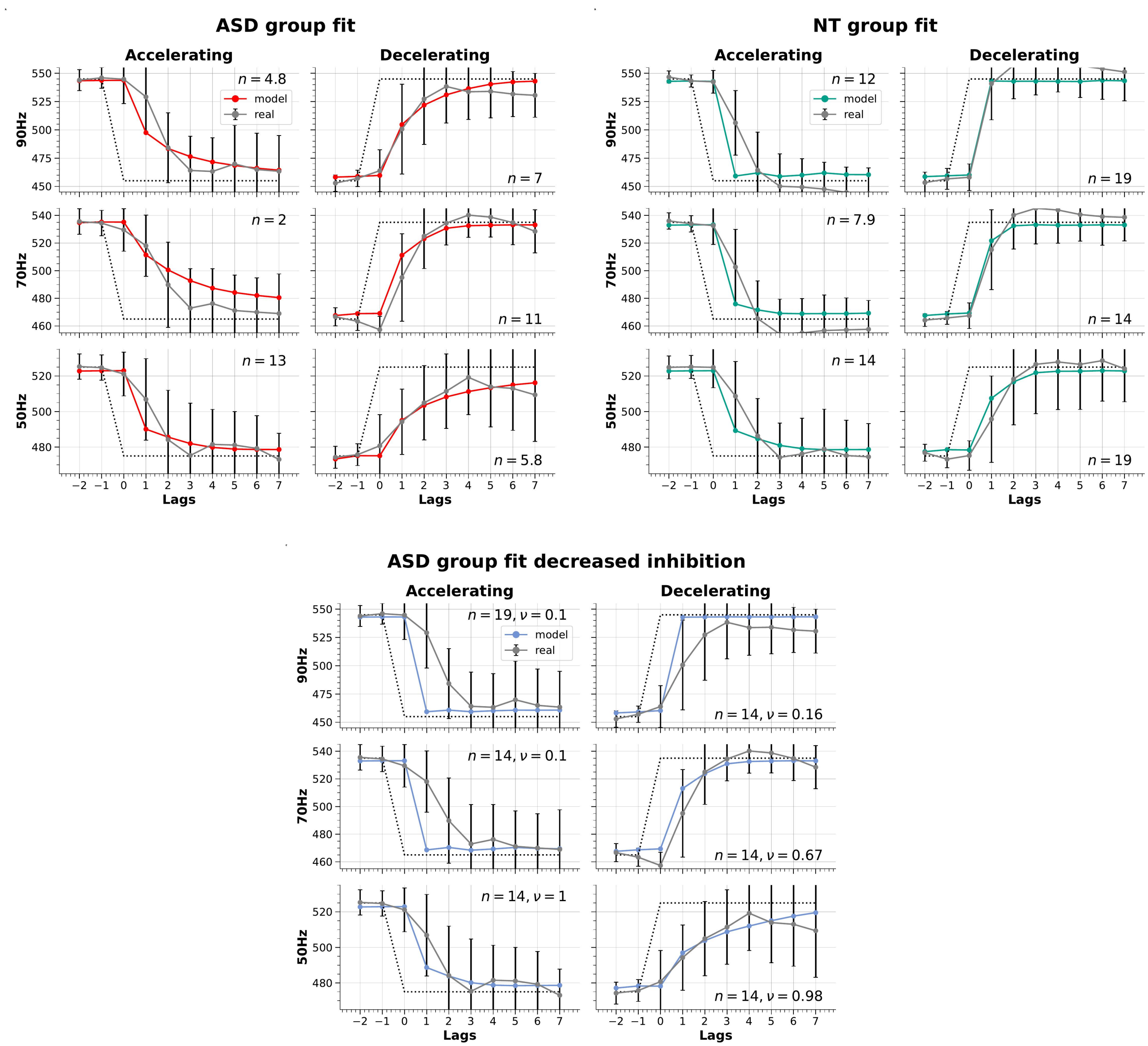

Supplementary Figure 26: **Group level fits for increased dynamic range model for the ASD and NT group data, and increased E/I ratio model for the ASD group data.** We fit the ASD and NT group-average tracking dynamics with the increased dynamic range model, and the ASD group data also with the increased E-I ratio model. The dynamic range model fits resulted in lower Hill-coefficients for the group level. Hill coefficients mean±ste, ASD: 7.4 ± 0.1, NT: 14 ± 0.1. Fitting the ASD group with increased E/I ratio resulted in Hill coefficients mean±ste: 15 ± 1.7. The mean MSE of the dynamic range model for the ASD group: 66, increased dynamic range for the NT group: 127 and for the increased E/I ratio model with the ASD group: 169. Note that the only block with fitted $\nu = 1$, is the accelerating 50Hz step block. The encoding of this frequency is 0.66, which exhibits the same levels of encoding variance for the increased excitation-inhibition ratio model with low and high Hill-coefficients (see main text Fig. 2). Thus, there is a high Hill-coefficient parameter that matches the encoding variance level of the low hill coefficient parameter at this level and a $\nu = 1$ fit becomes possible.

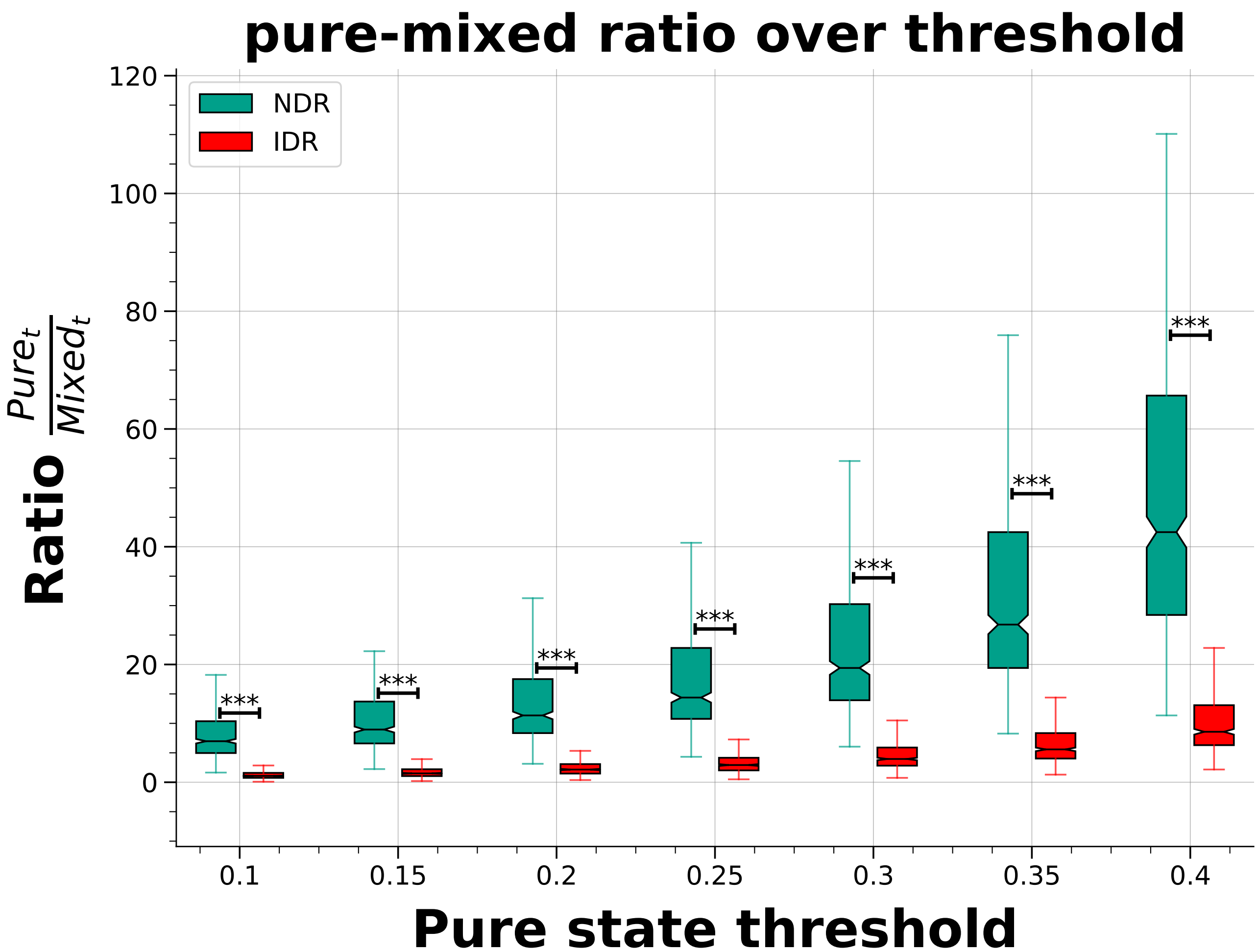

Supplementary Figure 27: **Sensitivity analysis for different threshold values for pure states in the binocular rivalry task.** Box centers are medians, minima and maxima are Q1, Q3 values, whiskers extend to the furthest data point that is within 1.5 times the inter-quantile range. Significance is marked by $'* < 0.5, ** < 0.01, *** < 0.001$.

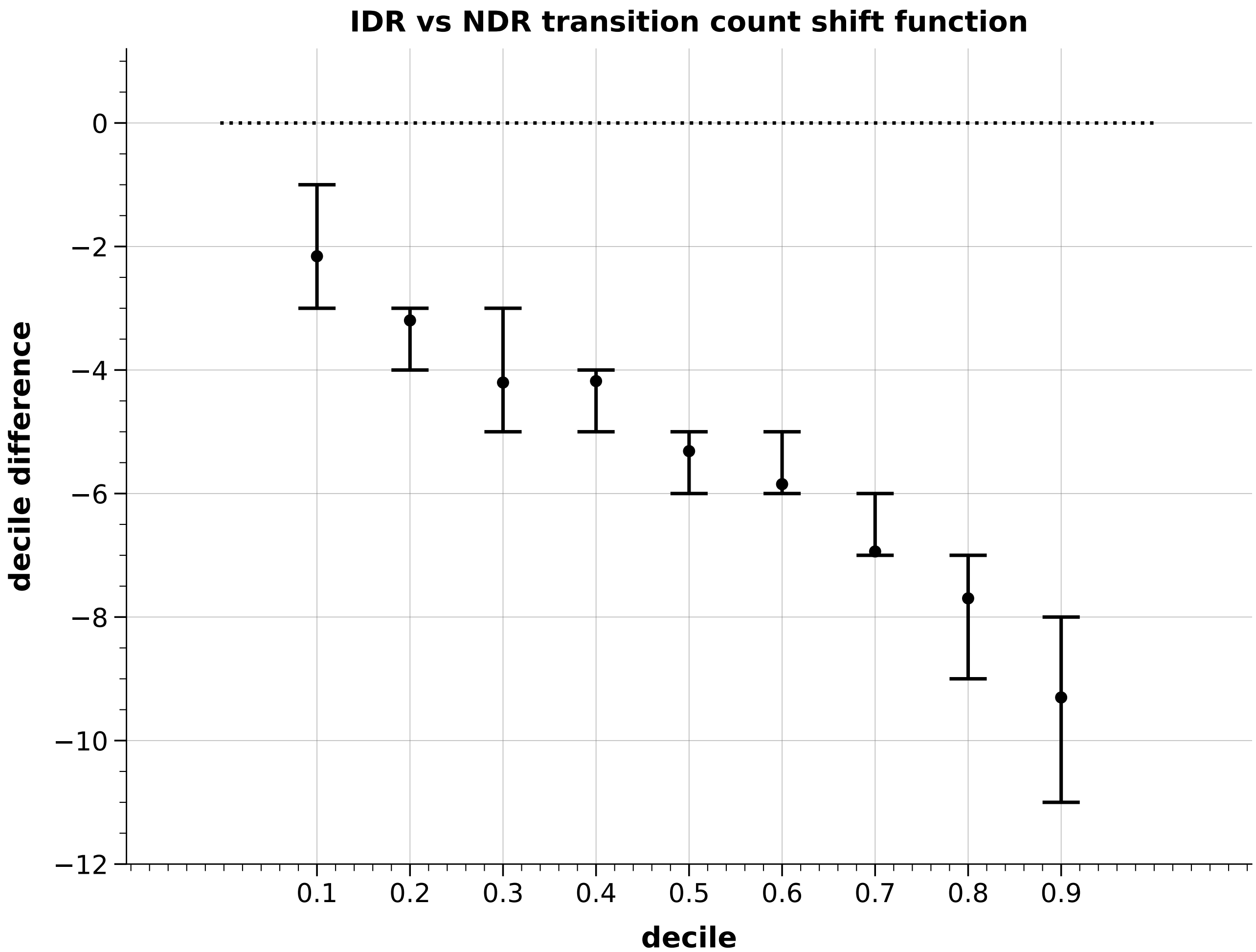

Supplementary Figure 28: **Shift function for increased vs. narrow dynamic range (IDR-NDR) distributions of state transition counts in binocular rivalry.** Comparison of distribution decile difference, black error-bars indicate 95% CI calculated via bootstrapping (10,000 samples).

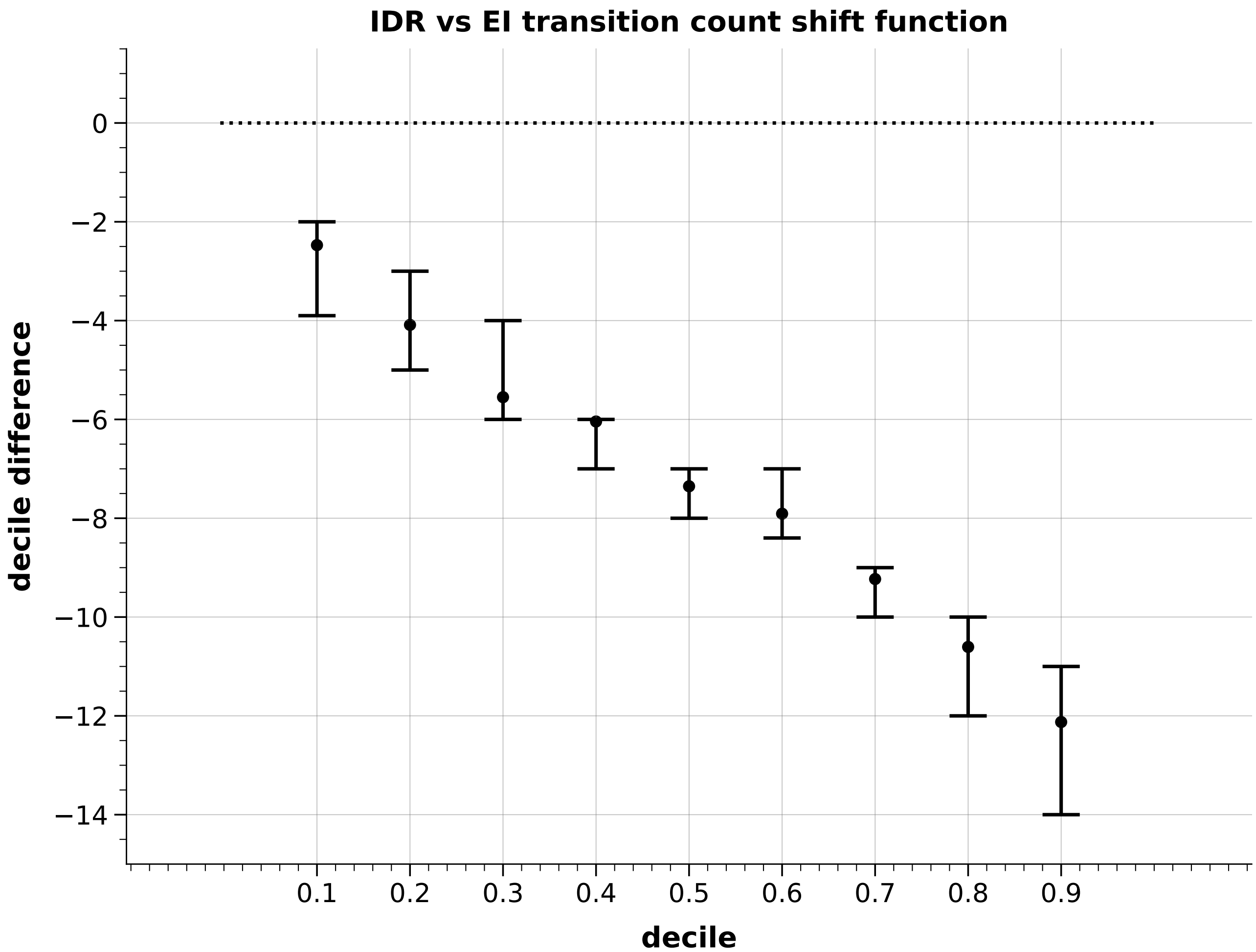

Supplementary Figure 29: **Shift function for increased dynamic range (IDR) vs. E-I imbalance model distributions of state transition counts in binocular rivalry.** Comparison of distribution decile difference, black error-bars indicate 95% CI calculated via bootstrapping (10,000 samples).

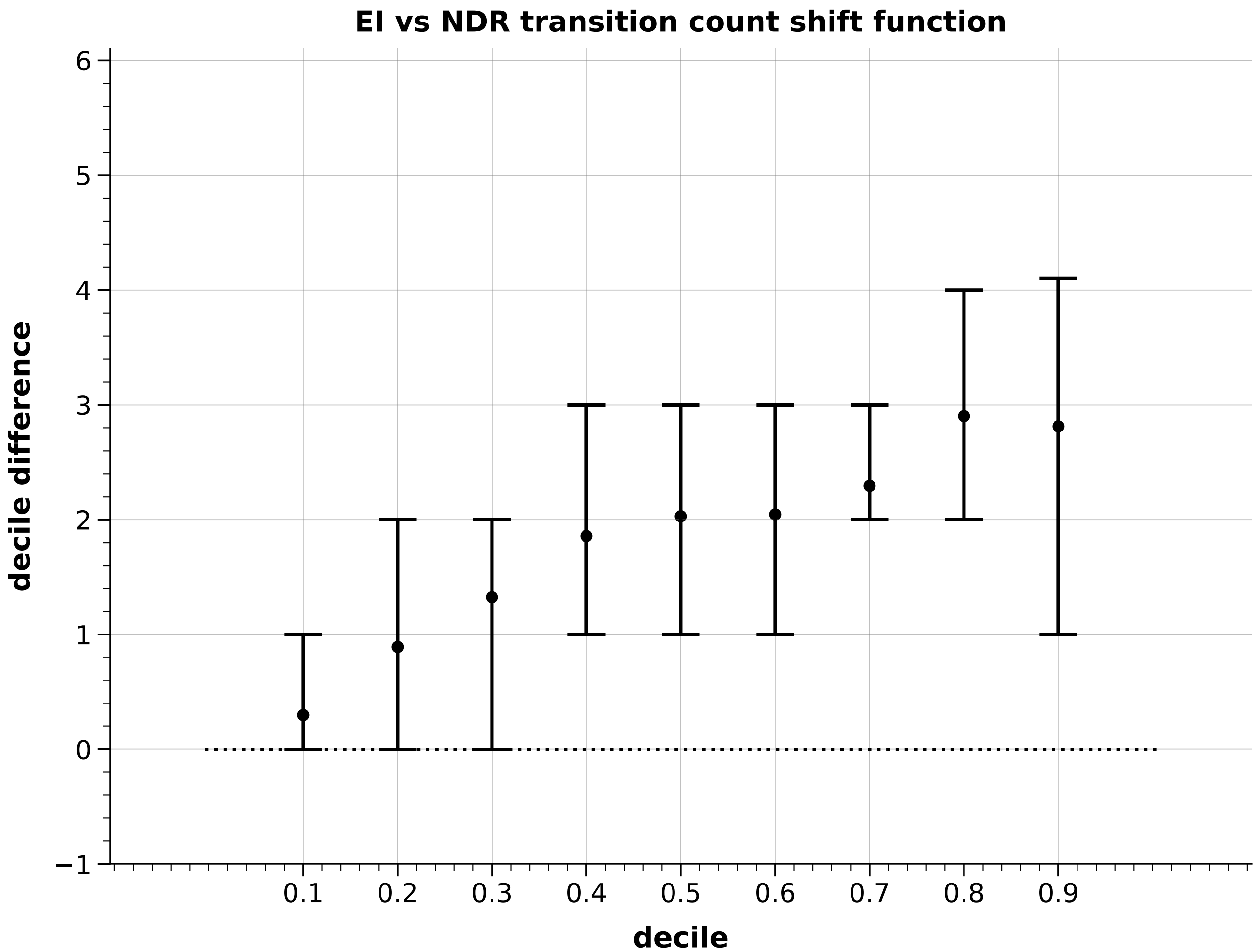

Supplementary Figure 30: **Shift function for E-I imbalance model vs. narrow dynamic range (NDR) distributions of state transition counts in binocular rivalry.** Comparison of distribution decile difference, black error-bars indicate 95% CI calculated via bootstrapping (10,000 samples).

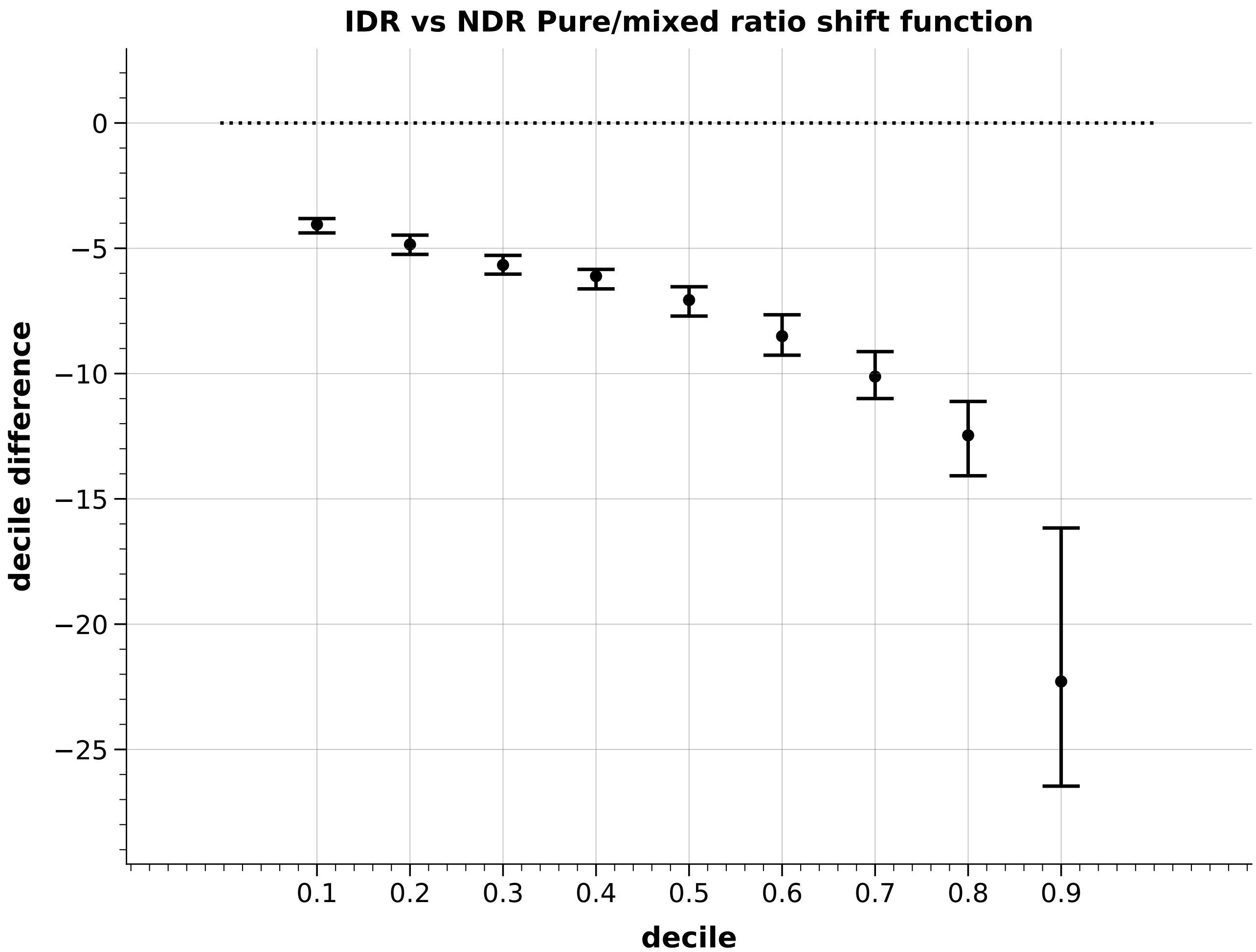

Supplementary Figure 31: **Shift function for increased vs. narrow dynamic range (IDR-NDR) distributions of pure-mixed states ratio in binocular rivalry.** Comparison of distribution decile difference, black error-bars indicate 95% CI calculated via bootstrapping (10,000 samples).

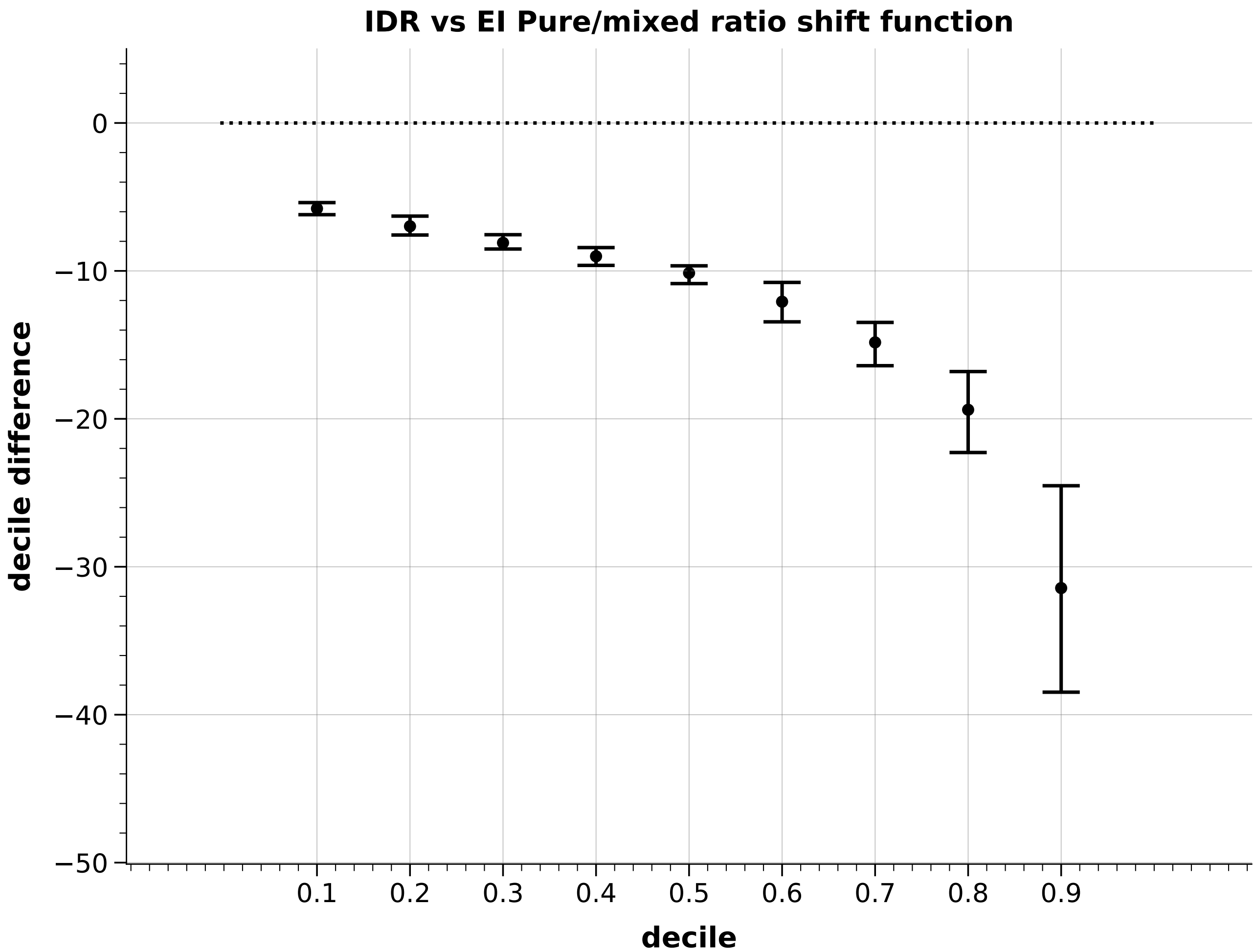

Supplementary Figure 32: **Shift function for increased dynamic range (IDR) vs. E-I imbalance model distributions of pure-mixed states ratio in binocular rivalry.** Comparison of distribution decile difference, black error-bars indicate 95% CI calculated via bootstrapping (10,000 samples).

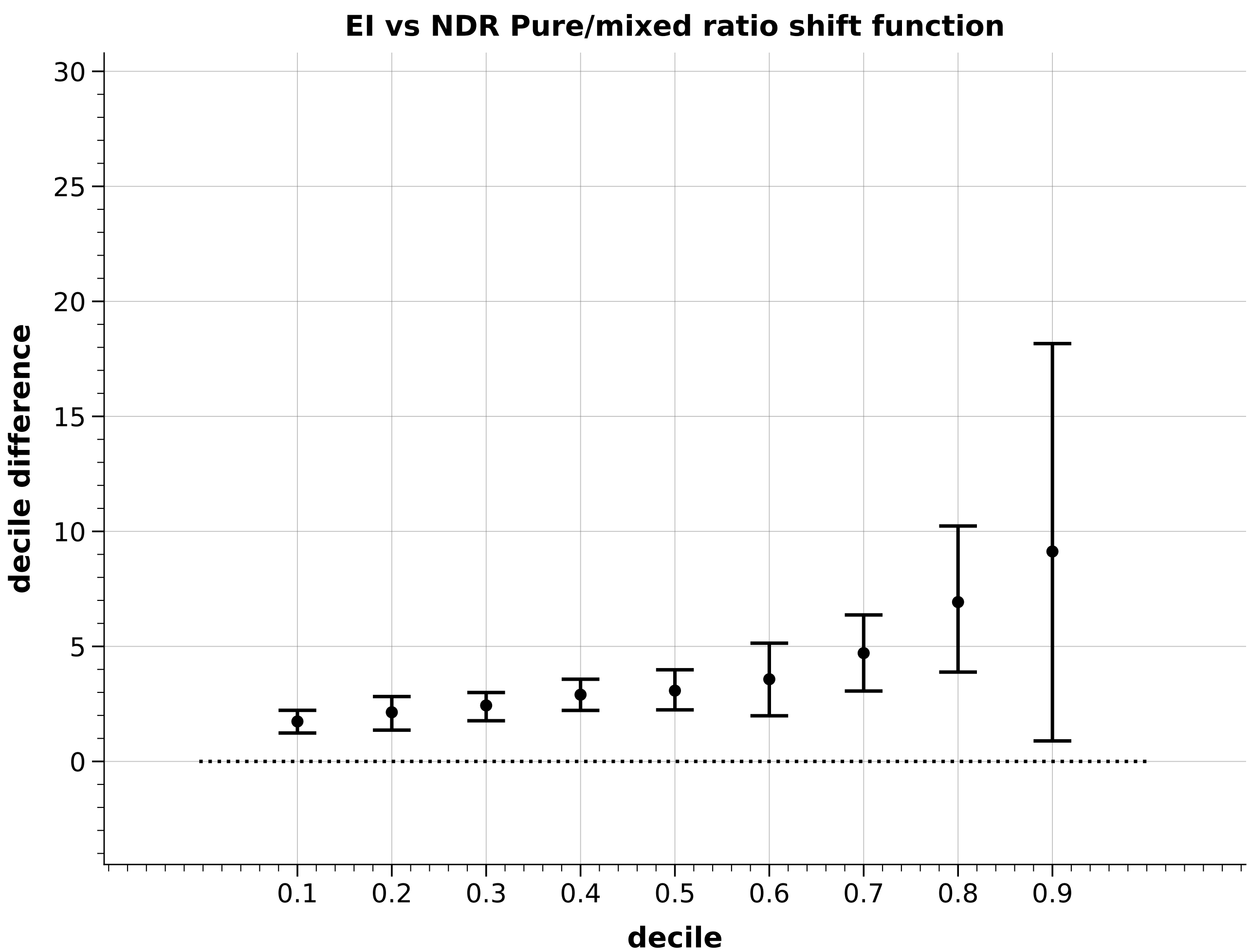

Supplementary Figure 33: **Shift function for narrow dynamic range (NDR) vs. E-I imbalance model distributions of pure-mixed states ratio in binocular rivalry.** Comparison of distribution decile difference, black error-bars indicate 95% CI calculated via bootstrapping (10,000 samples).

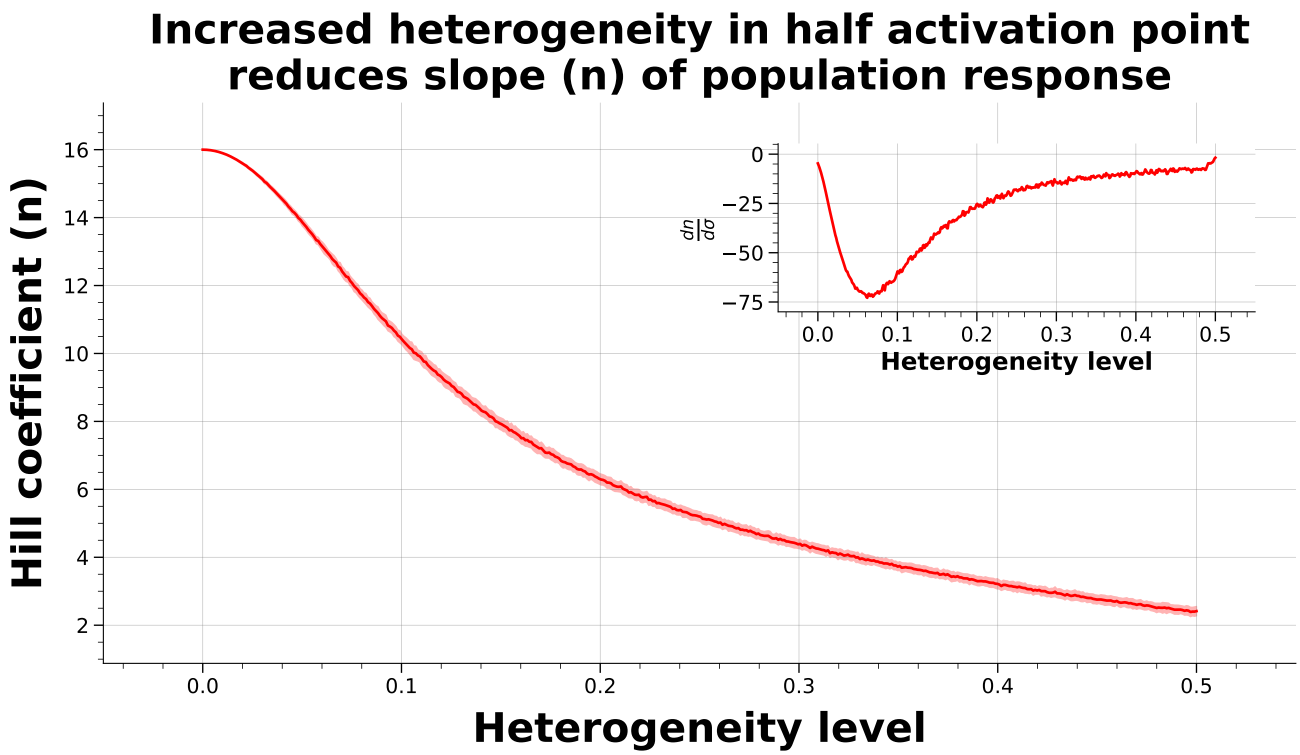

Supplementary Figure 34: **Increased heterogeneity in the half-activation point reduces the slope (n) of the population response. (Main panel)** The relationship between the slope (Hill coefficient) of the population and the heterogeneity in half-activation points of the neurons in the population, for a population of 300 individual neurons with $n = 16$. Data are presented as mean±SD. **(Inset)** Derivative of the population slope (Hill coefficient) as a function of heterogeneity in half-activation points of the neurons in the population. Data are presented as mean±SD.

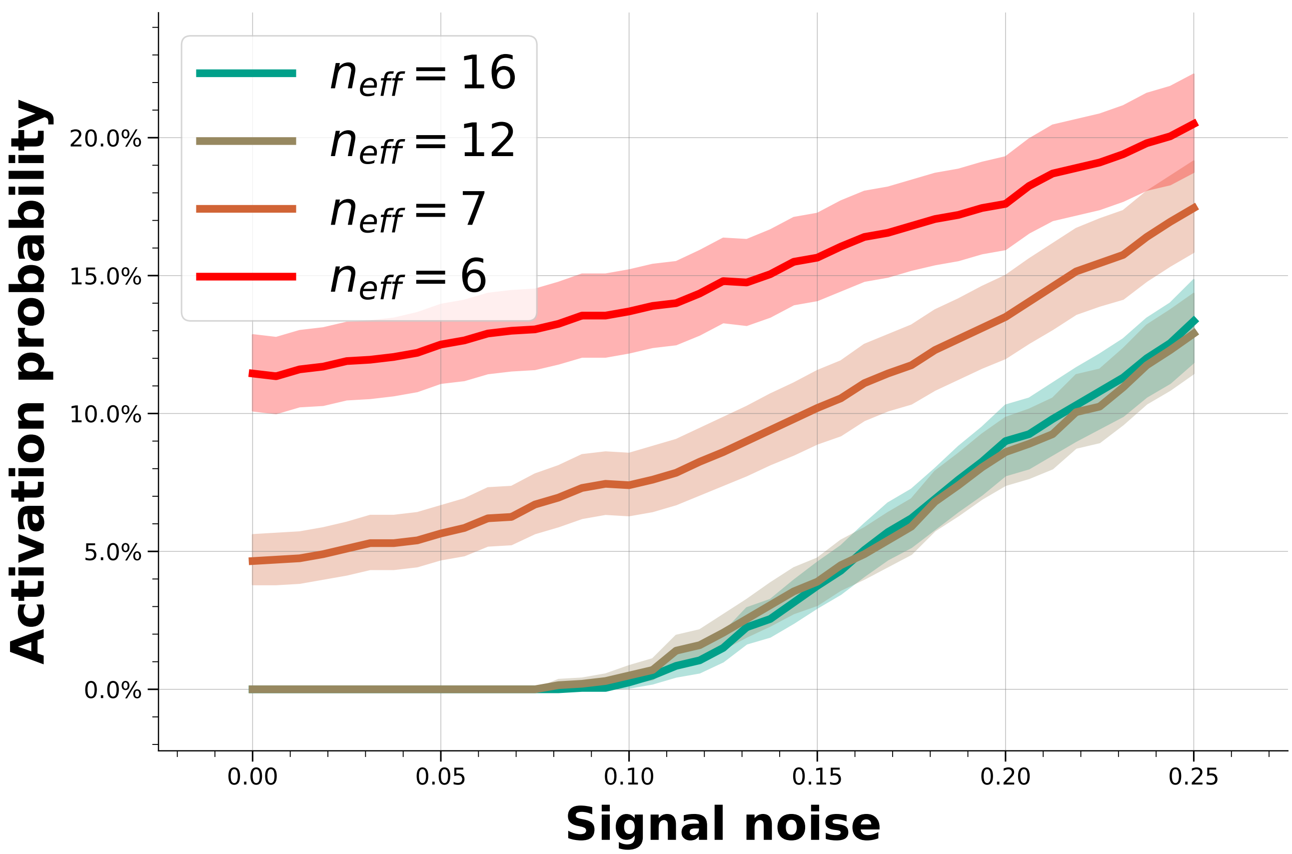

Supplementary Figure 35: **Heterogeneity in the population activity lowers the separatrix of the dynamical system, causing full activation for signal levels that should not activate the entire network.** Simulation results with an initial input signal level of 0.45. Extending the results in the main text, as the input signal level is closer to 0.5, the probability for spontaneous activation below the threshold becomes more prominent. Compare with the results of input signal set to 0.4 in the main text (Figure 8).

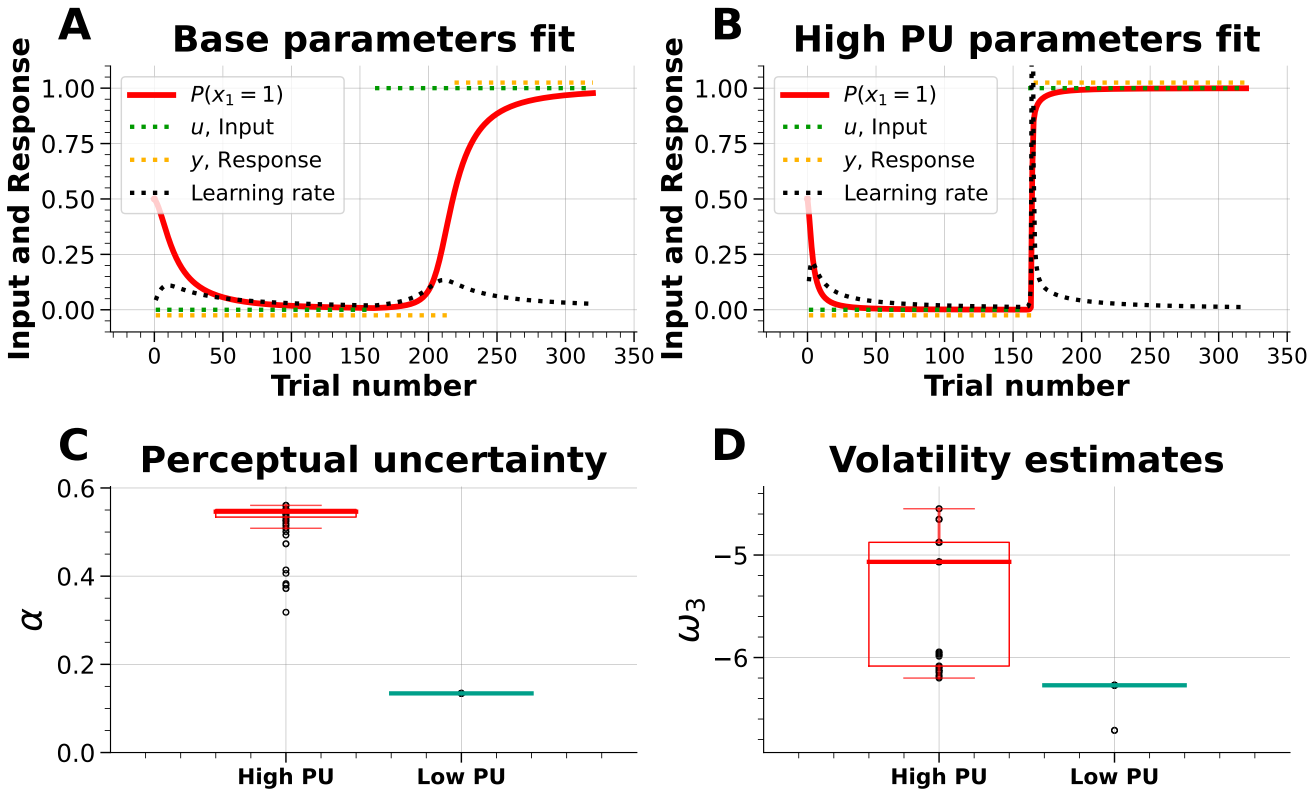

Supplementary Figure 36: **The higher perceptual variability of a gradual response increases volatility estimates.** Simulation of a binary Hierarchical Gaussian Filter[3] (HGF) with perceptual uncertainty (using the tapas implementation). Neurotypical (NT) parameters were retrieved using the default configuration of the model ("tapas_hgf_binary_pu_config") and "tapas_bayes_optimal_binary_config" observation model for an input signal (u) consisting of 160 steps of "0" followed by 160 steps of "1". The NDR parameters fitted for this model had perceptual uncertainty (PU) of $\alpha = 0.1341$. We generated responses from a model with an increased perceptual uncertainty (PU), akin to the gradual neuronal response (see Fig. 2 in the main text), by increasing the perceptual uncertainty to 0.6 and simulating the response of the model to the input u. We then extracted the fitting parameters to each of the simulations. Similar to previous results by Lawson et al.[4], increasing the perceptual uncertainty decreases ω_2 (uncertainty about probabilities) and increases ω_3 (volatility estimates) in the fitted model parameters, as well as decreases the learning rate at the time of signal change. **(A)** Input (green dots), trajectory of responses (orange dots), learning rate (black line) and the $s(\mu_2)$ expectation of the model (red line) with the base parameters (low PU, NDR-like). We find that $\omega_2 = -1.71$, $\omega_3 = -6.27$, and $\alpha = 0.134$. **(B)** Input (green dots), trajectory of responses (orange dots), learning rate (black line) and the $s(\mu_2)$ expectation of the model (red line) with a higher perceptual uncertainty. We find that for the high PU (IDR-like) condition $\omega_2 = -3.51$, $\omega_3 = -5.01$ and $\alpha = 0.55$. **(C)** Perceptual uncertainty estimates (α) are indeed higher for the higher perceptual uncertainty simulations. Low PU, NDR: Median $\alpha = 0.134$, 95% CI: $[0.134, 0.134]$, High PU, increased dynamic range (IDR): Median $\alpha = 0.546$, 95% CI: $[0.546, 0.548]$. The distribution of values relies on fits to 100 simulations with different random seeds. Centers represent median values, minima and maxima are Q1, Q3 values and whiskers extend to the farther data point within 1.5 times the inter-quantile range. **(D)** Volatility estimates (ω_3) are higher for the higher perceptual uncertainty simulations. Low PU, narrow dynamic range (NDR): Median $\omega_3 = -6.27$, 95% CI: $[-6.27, -6.27]$, High PU, increased dynamic range (IDR): Median $\omega_3 = -5.07$, 95% CI: $[-5.07, -4.88]$. The distribution of values relies on fits to 100 simulations with different random seeds. Centers represent median values, minima and maxima are Q1, Q3 values and whiskers extend to the farther data point within 1.5 times the inter-quantile range.

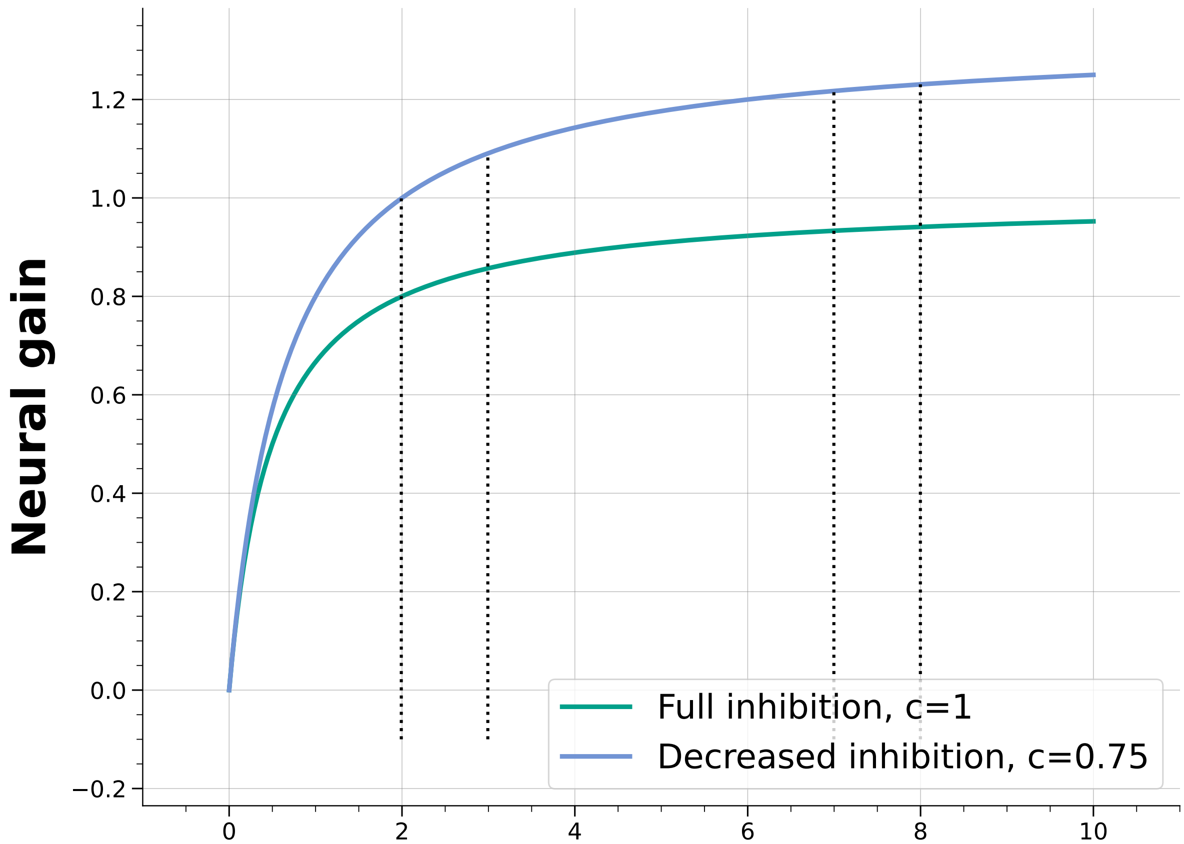

Supplementary Figure 37: **Replication of main text Fig. 1 using the encoding function of Rosenberg et al. 2015[1] to assess ASD to NT differences by changing the strength of the inhibition parameter, c.**

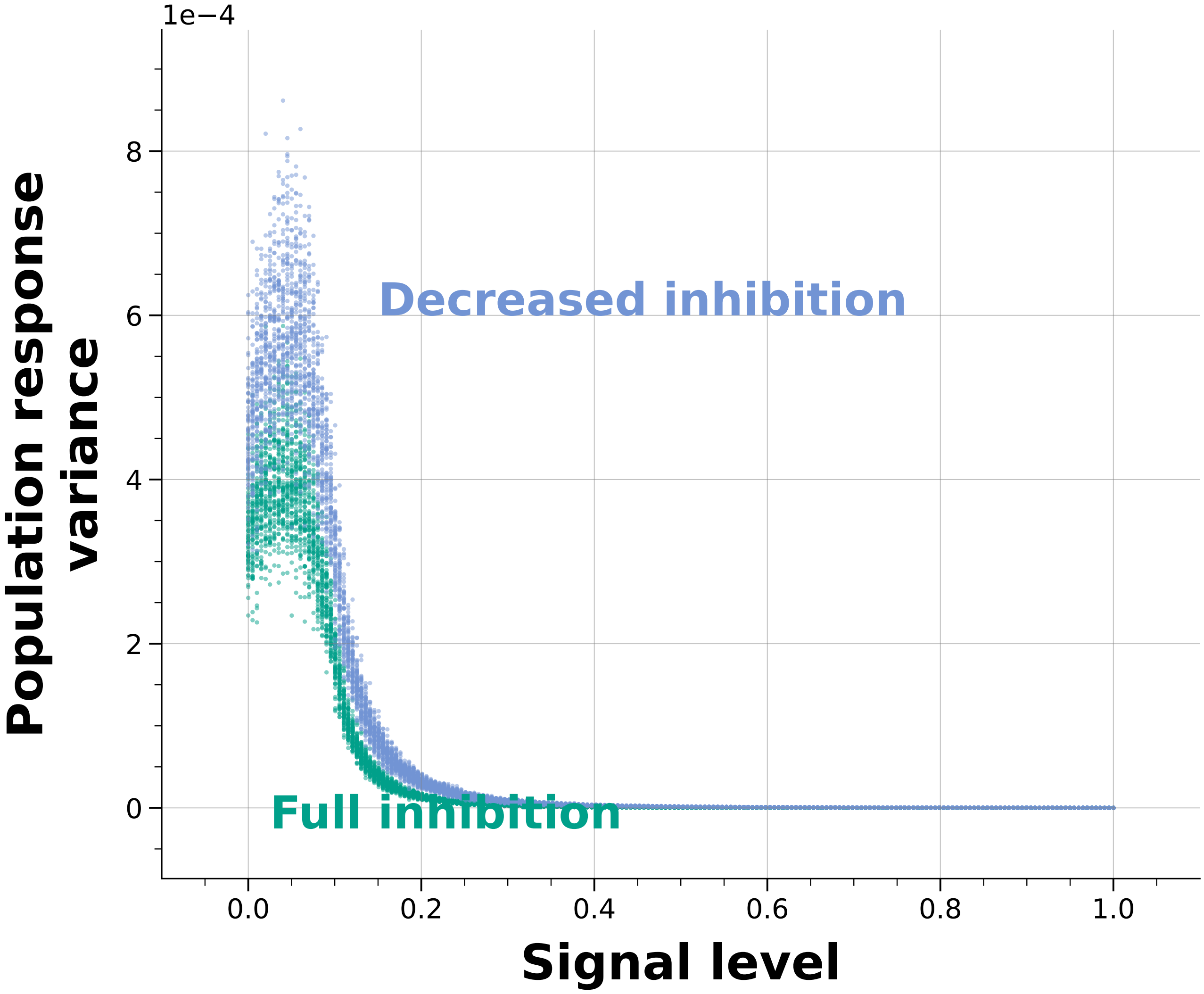

Supplementary Figure 38: **Replication of main text Fig. 2 using the encoding function of Rosenberg et al. 2015[1]**

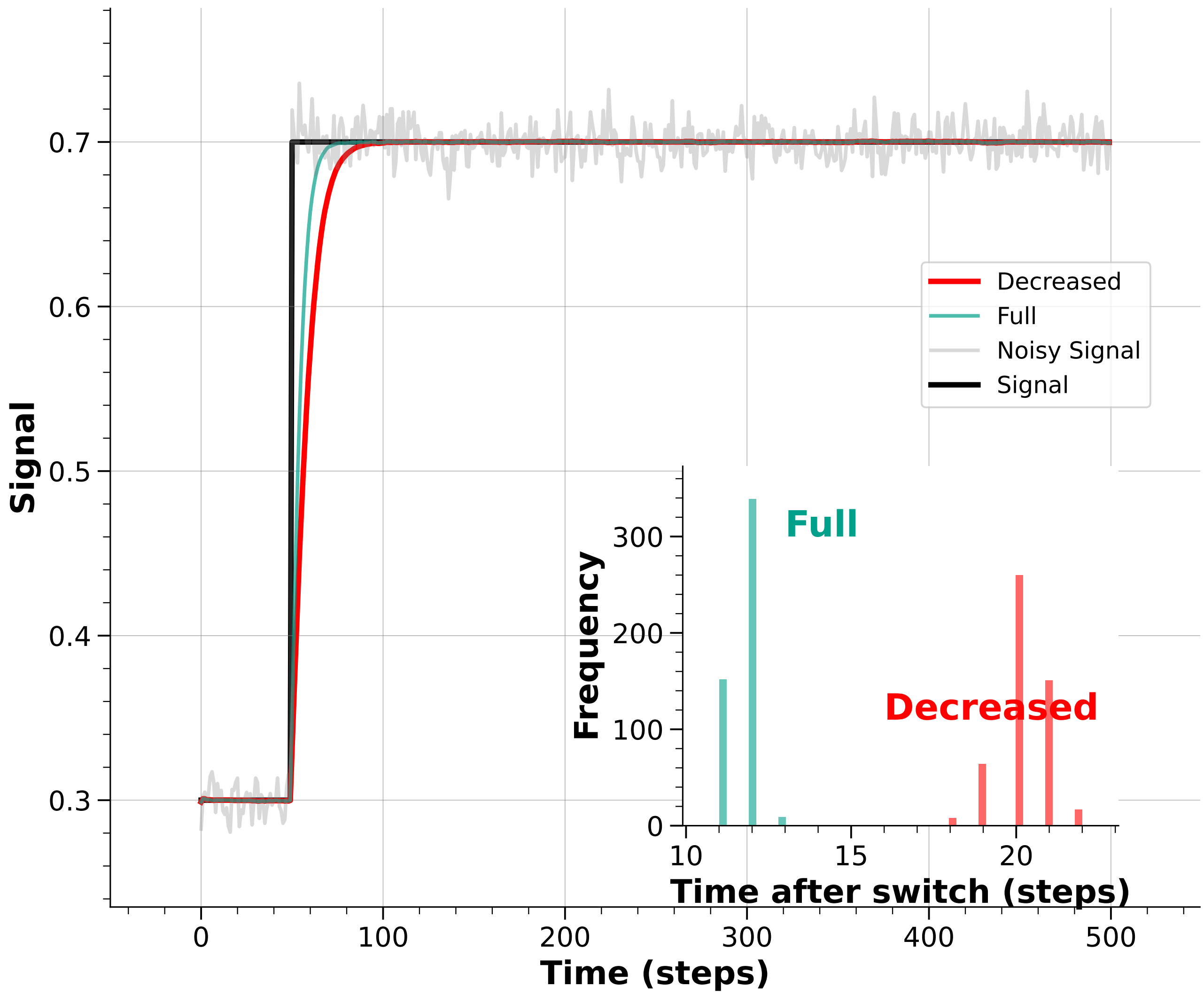

Supplementary Figure 39: **Replication of main text Fig. 3A using the encoding function of Rosenberg et al. 2015[1].**

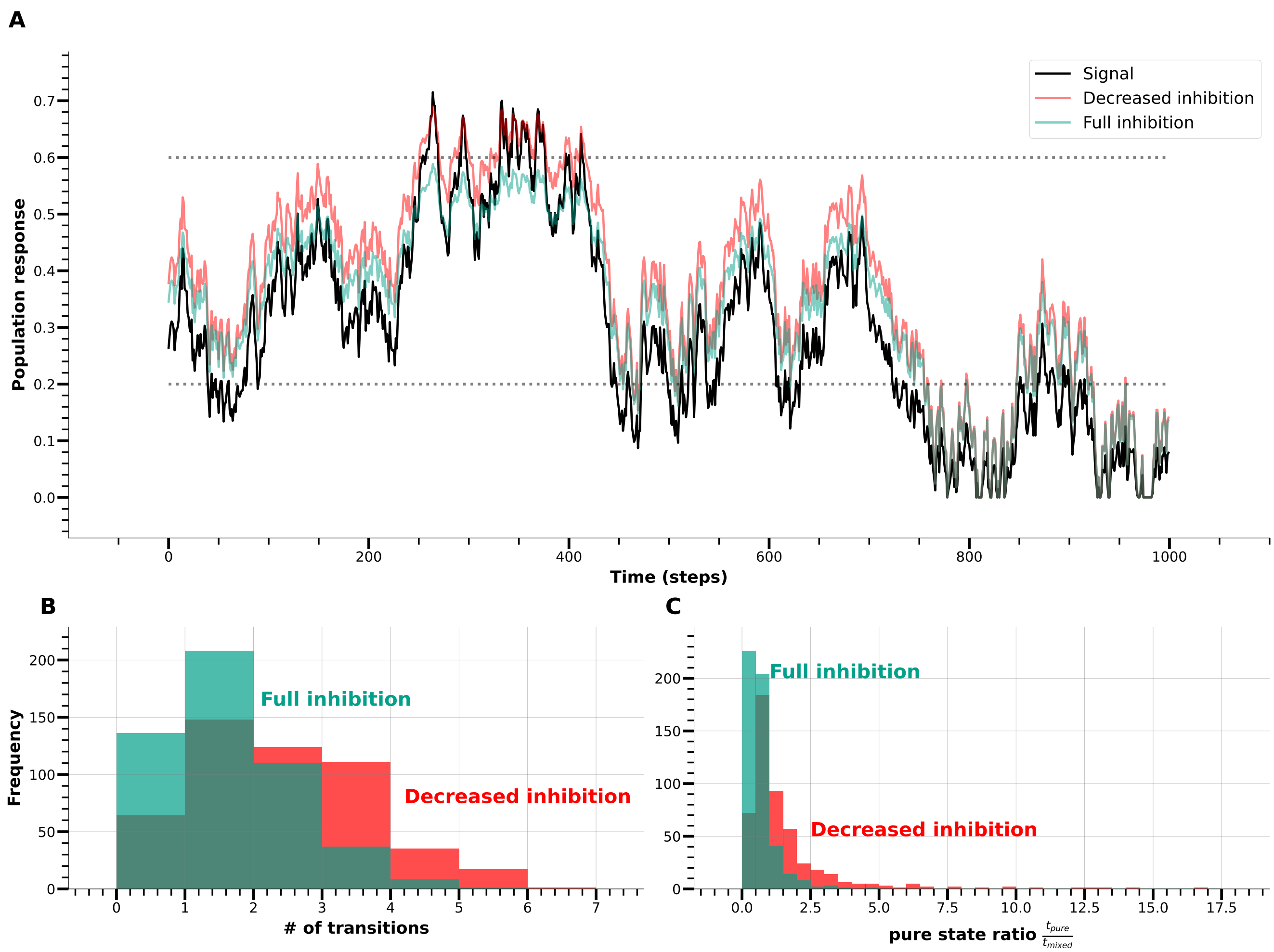

Supplementary Figure 40: **Replication of main text Fig. 4 using the encoding function of Rosenberg et al. 2015[1]. Note that decreased inhibition (simulating ASD-like behavior) shows higher transition rates and longer "pure" state durations, contrary to the experimental results.**

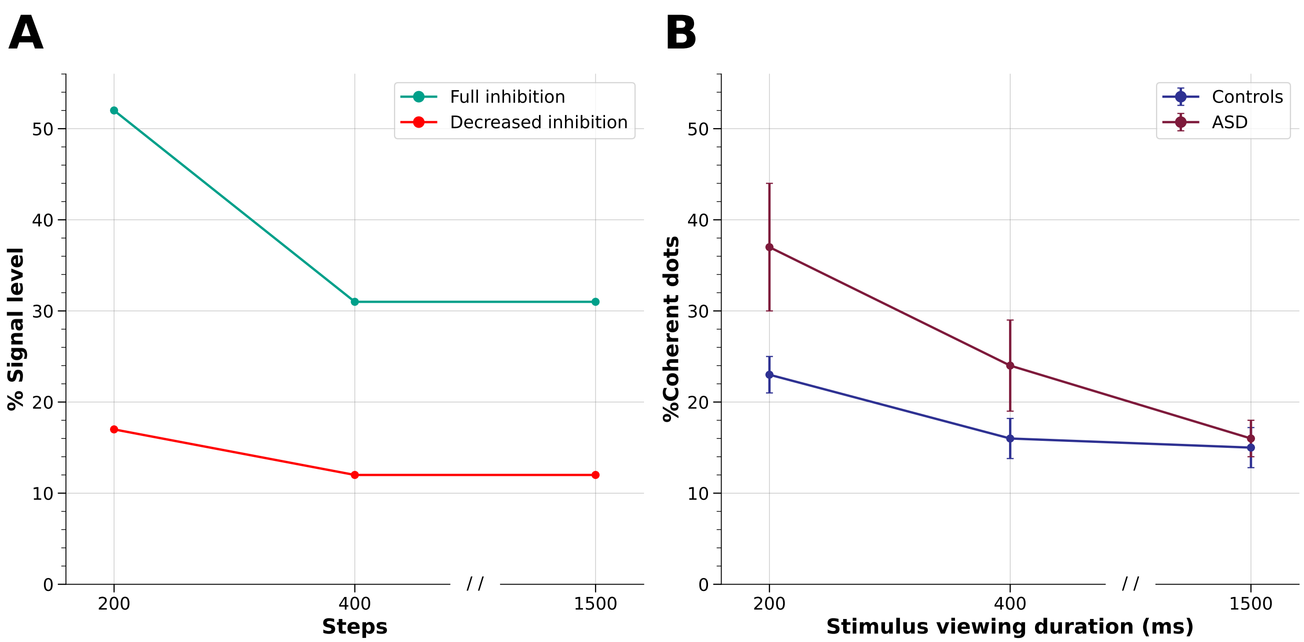

Supplementary Figure 41: **Replication of main text Fig. 5B-C using the encoding function of Rosenberg et al. 2015[1]. Note that contrary to the experimental results, decreased inhibition (simulating ASD-like behavior) shows lower thresholds for detection compared to regular inhibition (simulation NT).**

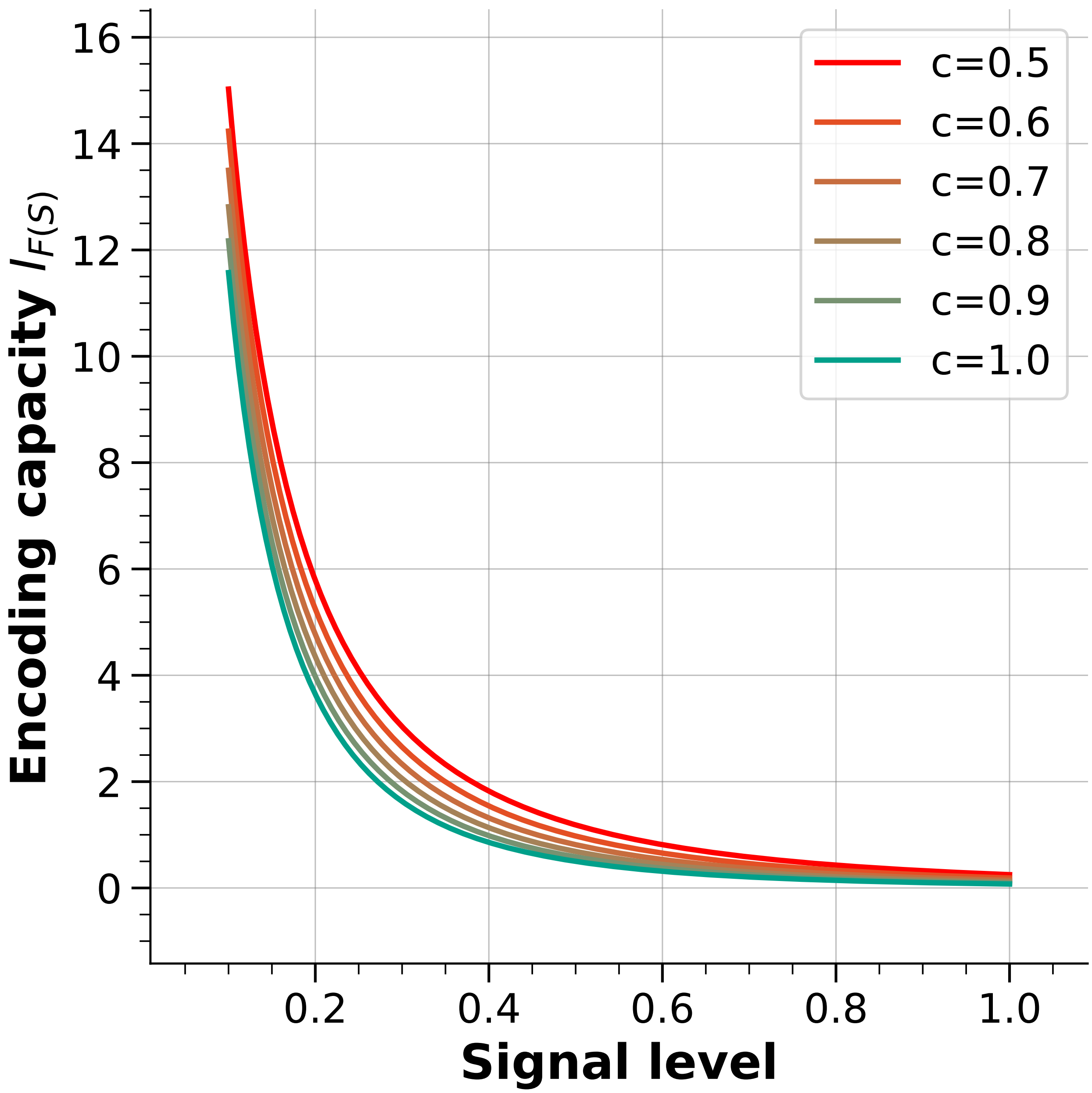

Supplementary Figure 42: **Replication of main text Fig. 6B using the encoding function of Rosenberg et al. 2015[1]. Note that contrary to the experimental findings, decreasing inhibition (thus simulating ASD-like behavior) increases the encoding capacity.**

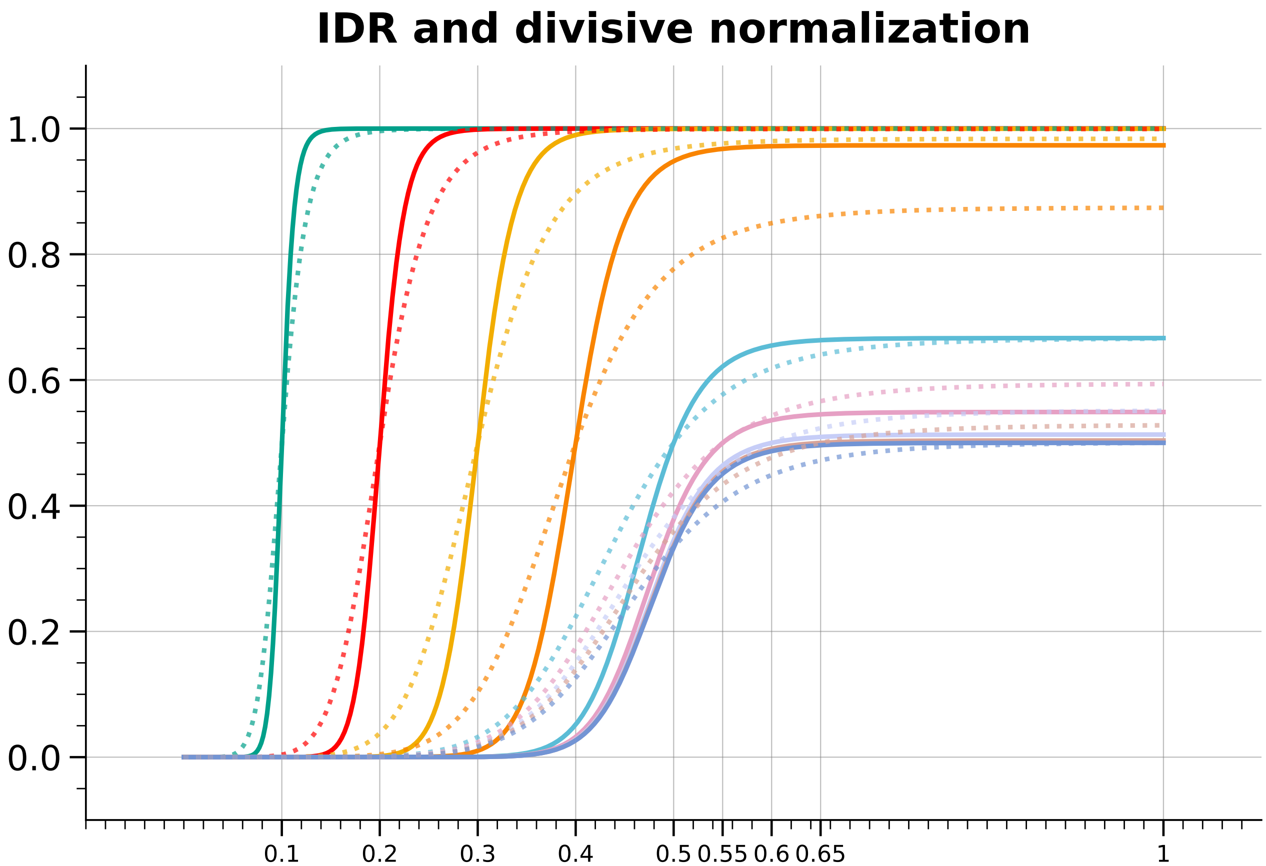

Supplementary Figure 43: **Divisive normalization and increased dynamic range (IDR).** Using the Hill-equation, the effects of increased dynamic range on outputs of divisive normalization on signals paired with one of the following signal levels: $[0.1, 0.2, 0.3, 0.4, 0.5, 0.55, 0.6, 0.65]$. Full lines are for Hill-coefficient, $n = 16$ (NDR), dashed lines for Hill-coefficient, $n = 8$ (IDR). $K_m = 0.5$ for all lines. Note that for signal levels above 0.5, IDR levels are higher than NDR, indicating an effective decreased inhibition. For signals lower than 0.5, IDR levels are either similar or below NDR levels, indicating comparable or stronger effective inhibition.

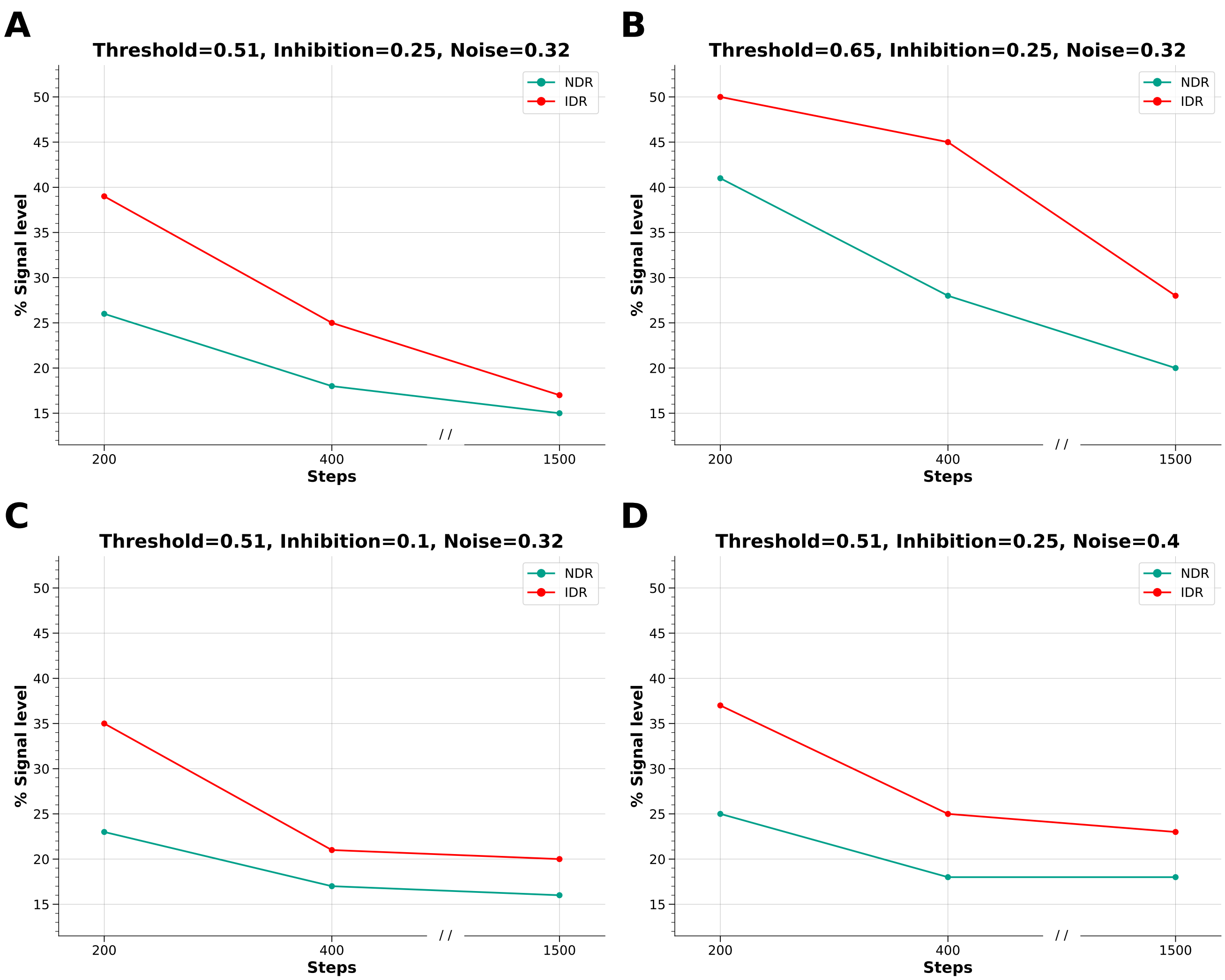

Supplementary Figure 44: **Effect of LCA parameters with Hill-equation encoding functions.** Comparison of increased dynamic range ($n = 8$) and narrow dynamic range ($n = 16$) in each panel. **(A)** Same parameters as the main text figure. **(B-D)** Each plot has one altered parameter from **A**.

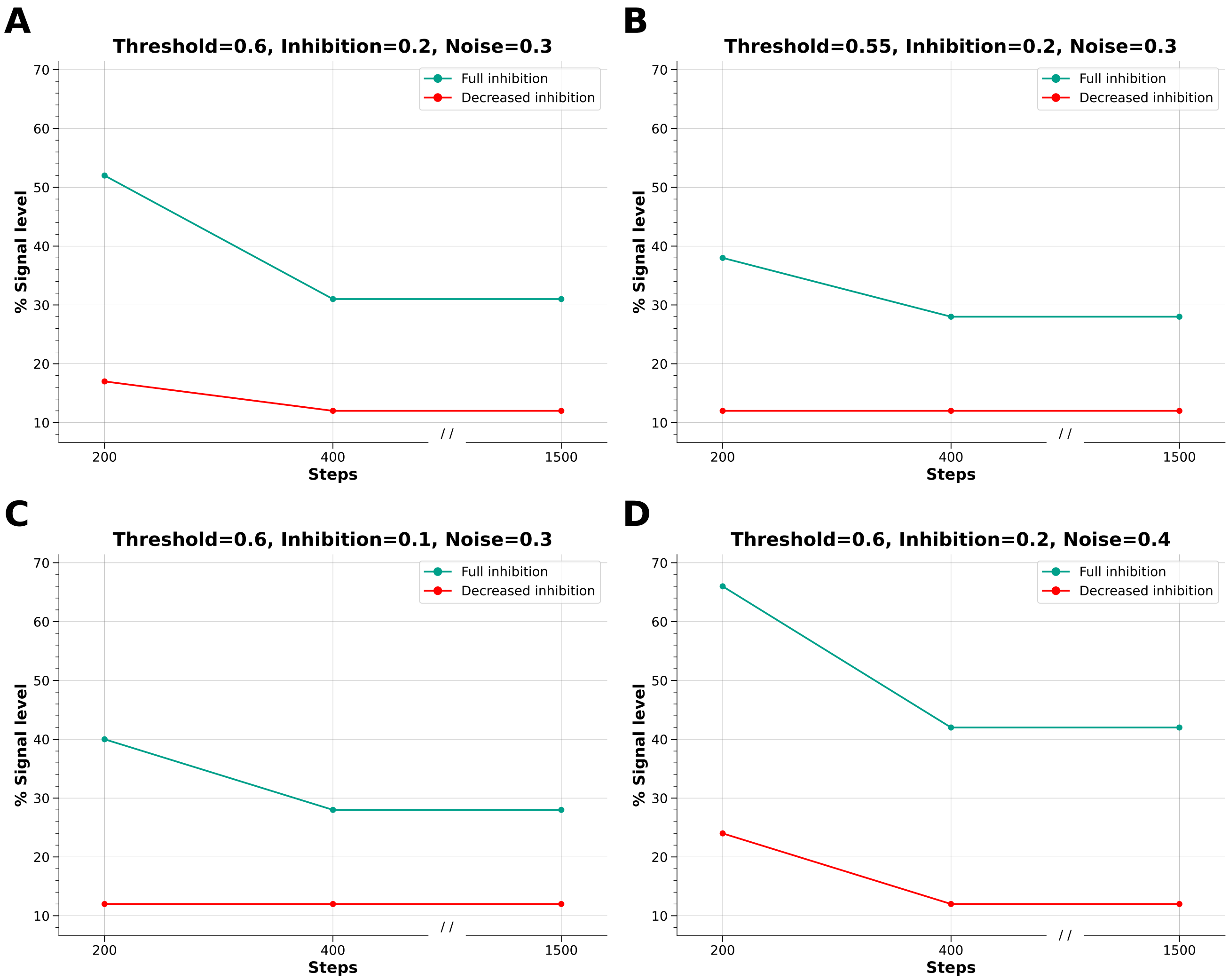

Supplementary Figure 45: **Effect of the Leaky, Competing Accumulator (LCA) parameters with Rosenberg et al. 2015 [1] divisive normalization equation with regular and decreased inhibition encoding functions.** Decreased inhibition is 75% of the regular inhibition.**(A)** Same parameters as the main text figure. **(B-D)** Each plot has one altered parameter from **A**.

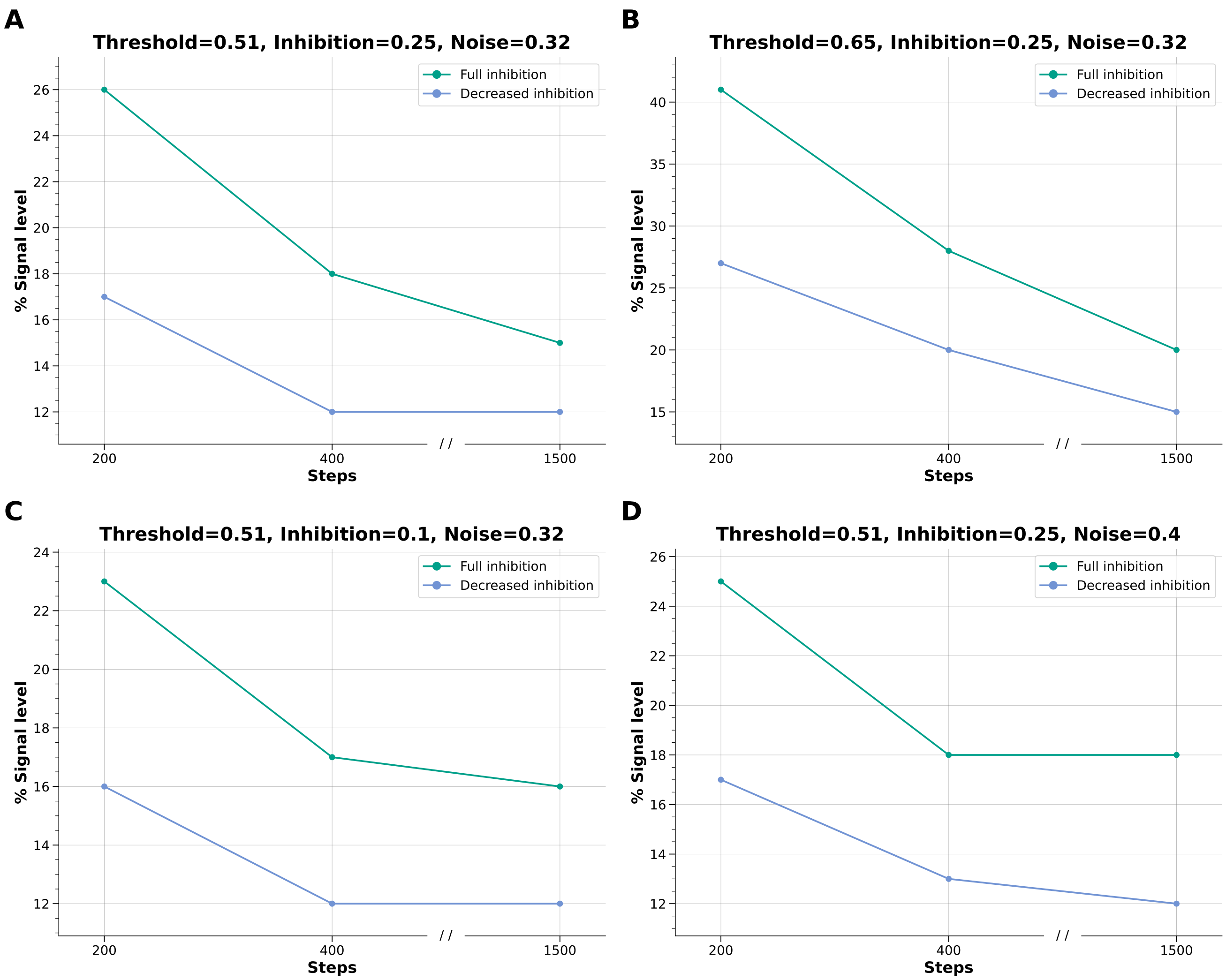

Supplementary Figure 46: **Effect of LCA parameters with Hill-equation encoding functions and decreased inhibition.** Comparison of narrow dynamic range with regular inhibition ($n = 16, \nu = 1$) and narrow dynamic range with decreased inhibition ($n = 16, \nu = 0.75$) in each panel. **(A)** Same parameters as the main text figure. **(B-D)** Each plot has one altered parameter from **A**.

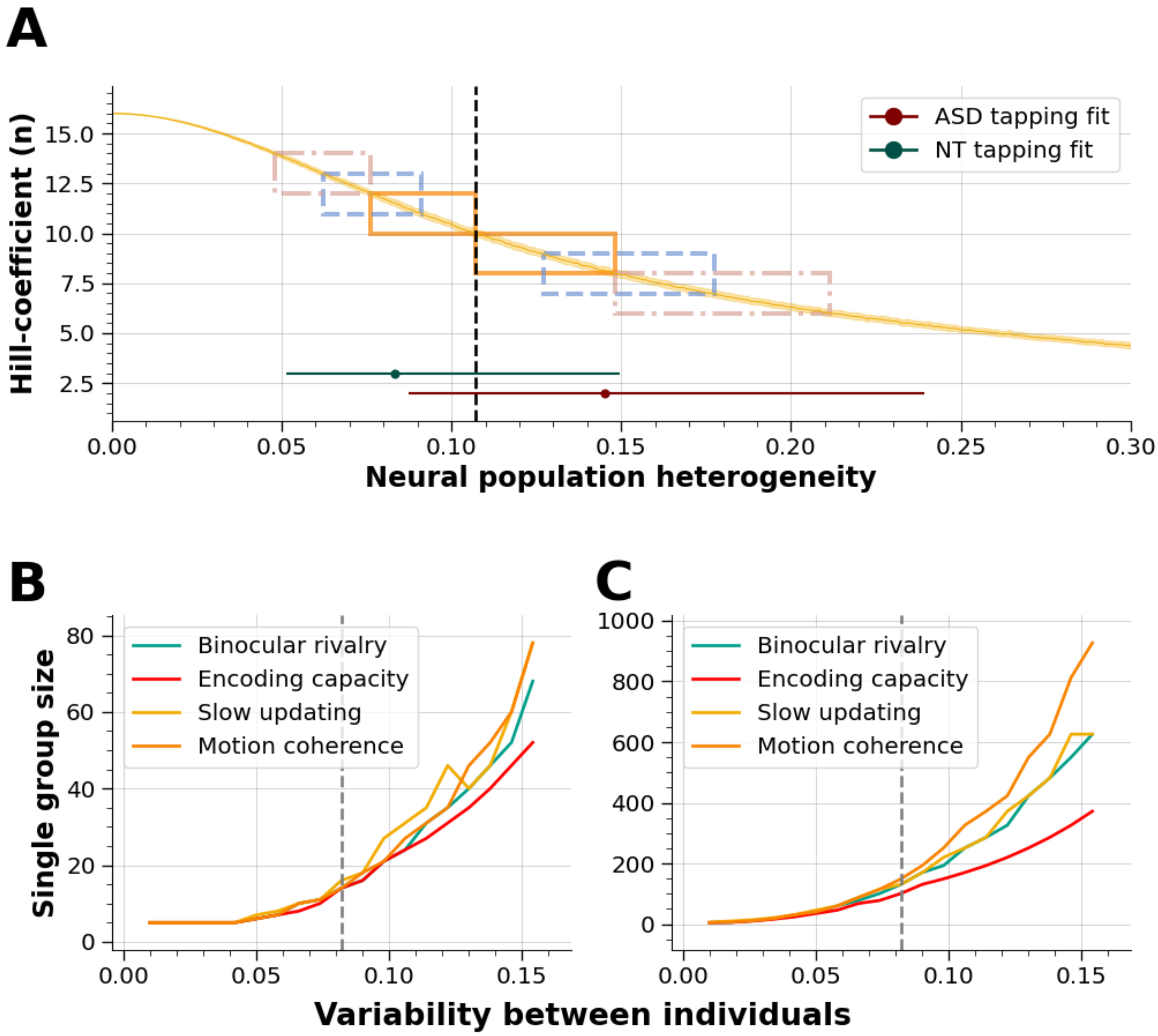

Supplementary Figure 47: Same as Extended Data Fig. 1 but with calculating the median (instead of the mean) heterogeneity level for each individual of their fitted Hill-coefficients in the tapping synchronization task. **(A)** The effect of neural within-population variability and dynamic range, illustrating different possible sub-samples of dynamic range levels of individuals in studies. Samples in different studies might probe many combinations of dynamic ranges in the ASD and NT groups, eliciting different effect sizes for any given task. In this illustration we take an arbitrary threshold determining ASD diagnosis - with dynamic ranges below $n = 10$ indicating an ASD diagnosis. We present three possible sampling scenarios - two well separated groups ($n_{ASD} = 7, n_{NT} = 13$, light purple boxes), two closer groups ($n_{ASD} = 8, n_{NT} = 12$, blue boxes), and two groups just across the arbitrary threshold ($n_{ASD} = 9, n_{NT} = 11$, orange boxes). The mean (circle) and the IQR (line) of the heterogeneity leading to the median fitted Hill-coefficients obtained in the tapping synchronization task are presented at the bottom of the panel in darker red (ASD) and turquoise lines (NT). **(B)** Power analysis for different simulated tasks for the scenario depicted in panel A, light purple boxes (mean Hill-coefficients $n_{IDR} = 7, n_{NDR} = 13$). Power analysis is presented for belief updating, binocular rivalry, motion coherence simulations and the encoding capacity calculation. Presented is the number of participants in each group (IDR/NDR) required to achieve 80% power in the simulated experiment. The dotted gray line indicates the level of variance between individuals from the median fitted Hill-coefficients of the tapping synchronization experiment data. **(C)** Same as panel B, for the scenario depicted in panel A, for the two groups just across the threshold, orange boxes (mean Hill-coefficients $n_{IDR} = 9, n_{NDR} = 11$).

References

[1] Rosenberg, A., Patterson, J. S. & Angelaki, D. E. A computational perspective on autism. *Proceedings of the National Academy of Sciences of the United States of America* **112**, 9158–9165, DOI: 10.1073/pnas.1510583112 (2015).

[2] Vishne, G. *et al.* Slow update of internal representations impedes synchronization in autism. *Nature communications* **12**, 5439 (2021).

[3] Mathys, C. D. *et al.* Uncertainty in perception and the hierarchical gaussian filter. *Frontiers in human neuroscience* **8**, 825 (2014).

[4] Lawson, R. P., Mathys, C. & Rees, G. Adults with autism overestimate the volatility of the sensory environment. *Nature neuroscience* **20**, 1293–1299 (2017).